HHS Public Access

Author manuscript

Nat Biomed Eng. Author manuscript; available in PMC 2019 September 04.

Published in final edited form as:

Nat Biomed Eng. 2019 April ; 3(4): 292–305. doi:10.1038/s41551-019-0360-0.

Depletion of PD-1-positive cells ameliorates autoimmune disease

Peng Zhao[1], **Peng Wang**[1], **Shuyun Dong**[1], **Zemin Zhou**[2], **Yanguang Cao**[3], **Hideo Yagita**[4], **Xiao He**[2], **Song Guo Zheng**[5], **Simon J. Fisher**[6], **Robert S. Fujinami**[2], and **Mingnan Chen**[1]

[1]Department of Pharmaceutics and Pharmaceutical Chemistry, University of Utah, Salt Lake City, UT 84112, USA

[2]Department of Pathology, University of Utah School of Medicine, Salt Lake City, UT 84112, USA

[3]Division of Pharmacotherapy and Experimental Therapeutics, the UNC Eshelman School of Pharmacy, University of North Carolina at Chapel Hill, Chapel Hill, NC 27599, USA

[4]Department of Immunology, Juntendo University School of Medicine, Tokyo, Japan.

[5]Division of Rheumatology, Department of Medicine, Penn State Milton S. Hershey Medical Center, Hershey, PA 17033, USA

[6]Division of Endocrinology, Metabolism, and Diabetes, Department of Internal Medicine, University of Utah, Salt Lake City, UT 84112, USA

Abstract

Targeted suppression of autoimmune diseases without collateral suppression of normal immunity remains an elusive yet clinically important goal. Targeted blockade of the programmed death-1 receptor (PD-1) — an immune checkpoint factor expressed by activated T cells and B cells — is an efficacious therapy for potentiating immune activation against tumours. Here, we show that an immunotoxin consisting of an anti-PD-1 single-chain variable fragment, an albumin-binding domain and *Pseudomonas* exotoxin targeting PD-1-expressing cells selectively recognizes and induces the killing of the cells. Administration of the immunotoxin to mouse models of autoimmune diabetes delays disease onset, and its administration in mice paralyzed by experimental autoimmune encephalomyelitis ameliorates symptoms. In all mouse models, the immunotoxin reduced the numbers of PD-1-expressing cells, of total T cells and of cells of an autoreactive T cell clone found in inflamed organs, while maintaining active adaptive immunity, as

Corresponding author: Mingnan Chen, Ph.D., Mailing address: 30 South 2000 East, Skaggs Pharmacy Hall, Room 301, Salt Lake City, UT 84112, USA, Phone: (+1) 801-581-7616, mingnan.chen@utah.edu.

AUTHOR CONTRIBUTIONS:

P.Z. and M.C. wrote the manuscript with significant suggestions from Z. G. S, S.J.F. R.S.F. P.Z. and M.C. designed all experiments and analyzed all experimental data. Additionally, S.J.F. and X.H. contributed to the design of the T1D studies; R.S.F. contributed to the design of the EAE studies; Z.Z. generated PD-1^{-} EL4 cells; Y.C. assisted in PK analysis. P.Z. design and prepared immunotoxin with an assistance from S.D. P.Z. characterized immunotoxin *in vitro* and *in vivo*. P.W. contributed to the design of ABD and the related studies. H.Y. provided the aPD-1 hybridoma and guidance about PD-1 biology. All authors discussed the results and commented on the manuscript.

COMPETING INTERESTS

M.C., P.Z. and P.W. have a pending patent application related to this work.

evidenced by full-strength immune responses to vaccinations. The targeted depletion of PD-1-expressing cells contingent to the preservation of adaptive immunity might be effective in the treatment of a wide range of autoimmune diseases.

Autoimmune diseases are primarily mediated by auto-reactive lymphocytes and/or their secreted auto-antibodies[1–4]. Targeted suppression of certain lymphocyte populations is an effective strategy to treat the diseases that has yielded new therapies for multiple sclerosis (MS) and systemic lupus erythematosus (SLE)[5–8]. However, these therapies are rarely considered as first-line therapeutic options due to their indiscriminate inhibition of normal adaptive immunity[6, 9–12]. This inhibition occurs because these therapies target lymphocytes too broadly [4–6, 11]. Thus, identification and selective suppression of pathogenic lymphocytes responsible for autoimmune diseases while keeping non-pathologic lymphocytes intact constitute an overarching yet unmet clinical goal.

PD-1$^+$ cells are primarily activated B and T cells or B and T effector cells[13–15]. PD-1, a negative receptor on these cells, switches on the PD-1 immune checkpoint when engaged by its ligands. This critical checkpoint counteracts immune stimulatory signals and limits PD-1$^+$ effector cells from initiating autoimmune destruction[16–23]. However, in type 1 diabetes (T1D), MS, SLE, and rheumatoid arthritis, the PD-1 checkpoint fails to stop autoimmune destruction[16, 21]. Instead, PD-1$^+$ cells infiltrate tissues[17, 19], and this infiltration escalates as the autoimmune diseases progress[19]. These observations indicate that PD-1$^+$ cells are important mediators of autoimmune diseases. Consistent with this concept, the blockade of the PD-1 checkpoint, which leads to a proliferation of PD-1$^+$ cells, exacerbates autoimmune diseases in both human and mouse models[19, 24–26]. Taken together, the targeted depletion of PD-1$^+$ cells (or PD-1$^+$ cell depletion) in the context of autoimmune diseases might be an effective method to assuage autoimmunity. It is worth mentioning that PD-1$^+$ cell depletion is a very different concept than ablation of the PD-1-gene. PD-1$^+$ cell depletion eliminates activated lymphocytes; in contrast, the knockout of the PD-1 gene leaves activated lymphocytes without control by the PD-1 checkpoint and allows for uncontrolled proliferation of activated lymphocytes[21]. Thus, whereas the knockout predisposes the host to enhanced autoimmunity, we hypothesize that PD-1$^+$ cell depletion suppresses autoimmunity.

There are two intrinsic advantages for using PD-1$^+$ cell depletion. First, the depletion should leave naïve lymphocytes (PD-1$^-$) intact and hence preserve B and T cell repertoires because the depletion primarily applies to activated lymphocytes. PD-1$^+$ cell depletion should not significantly compromise normal adaptive immunity, which distinguishes the depletion from current drugs used to treat autoimmune diseases such as natalizumab and alematuzumab[5, 6, 11]. Second, PD-1$^+$ cell depletion applies to both activated B and activated T cells since the both cells are PD-1-positive. The dual coverage of both activated B and T cells is advantageous because the both cells can contribute to autoimmune diseases[3].

Here, we describe αPD-1-ABD-PE as a tool for PD-1$^+$ cell depletion. This immunotoxin consists of a single-chain variable fragment (scFv) of αPD-1[27], an albumin-binding domain (ABD)[28, 29], and a Pseudomonas exotoxin (PE)[30, 31]. The αPD-1 scFv serves as a targeting moiety. The ABD is used to extend plasma presence of αPD-1-ABD-PE because ABD-

containing molecules have long plasma half-lives[28, 29, 32]. The PE has demonstrated to have clinical efficacy and is safe[30, 33]. αPD-1-ABD-PE possesses selective toxicity, both *in vitro* and *in vivo*, to PD-1$^+$ cells. More importantly, αPD-1-ABD-PE not only halted the progression of autoimmune diseases in our system, but also concomitantly preserved normal adaptive immunity.

Results

αPD-1-ABD-PE selectively binds and penetrate PD-1$^+$ cells

αPD-1-ABD-PE has three functional components: αPD-1 (scFv), ABD, and PE (Figure 1a). The sequences of the ABD and PE have been previously published[31, 34]. We sequenced an αPD-1 clone, RMP1–14, which is a rat anti-mouse PD-1 mAb (IgG2a, κ) [35]. Based on the sequencing results, we designed the αPD-1 to contain two mutations, V_H R45C and V_L G104C (Figure 1b). These two cysteines were introduced to form a disulfide bond and enhance stability of the αPD-1[36]. A linker, $(GGGGS)_3$, was used to connect the αPD-1, the ABD, and the PE. Three control proteins were also designed for our study: αPD-1, ABD-PE, and αPD-1-PE (Figure 1a). All of these proteins have a histidine-tag (HisTag) to facilitate purification. The coding genes for αPD-1-ABD-PE and the controls were cloned into pET25b (+) vector. The sizes of these genes were confirmed by agarose gel electrophoresis (Figure S1a). These genes were sequenced and confirmed to have the designed sequences. αPD-1-ABD-PE and the controls were produced and purified as soluble proteins from *E. coli* (Shuffle T7) that harbored the expression vectors. The yield was approximately 0.3 mg/L culture for each of these proteins. The purity and size of these proteins were examined by SDS-PAGE (Figure S1b). The sizes of these proteins reflected by SDS-PAGE results were consistent with their predicted theoretical molecular weights; e.g. αPD-1-ABD-PE migrated slightly lower than the 63 kDa marker, which was agreed with its theoretical molecular weight, 57.9 kDa. Endotoxin were removed from all purified proteins to levels below 0.1 unit/mg protein.

We found that αPD-1-ABD-PE selectively binds to PD-1$^+$ cells according to our results with three pairs of PD-1$^+$ and PD-1$^-$ cells: PD-1$^+$ and PD-1$^-$ primary T cells, PD-1$^+$ and PD-1$^-$ primary B cells, EL4 (PD-1$^+$)[37] and B16 (PD-1$^-$) cells (Figure S2a-b). We incubated Alexa Fluor 647-labeled αPD-1-ABD-PE with PD-1$^+$ and PD-1$^-$ cells, separately at 4°C (30 min) whereby cell surface binding was allowed but internalization by cells was inhibited. After the incubation, the mean fluorescence intensity (MFI) of the PD-1$^+$ primary T cells was more than 4 times of that of PD-1$^-$ primary T cells (188.33 ± 5.92 versus 43.45 ± 2.98; Figure 1c); the MFI of the PD-1$^+$ primary B cells was more than 5 times of that of PD-1$^-$ primary B cells (229.67 ± 12.45 versus 43.72 ± 2.46; Figure 1d); the MFI of EL4 cells was more than 3 times of that of B16 cells (571.70±12.12 versus 116.00±1.61; Figure S2c). In contrast, both the PD-1$^+$ and the PD-1$^-$ cells had low MFIs after similar incubations with labeled ABD-PE (Figure 1c-d, Figure S2c). Through a dose-responsive binding assay, we found that the apparent binding Kd of αPD-1-ABD-PE to PD-1$^-$ EL4 cells is 12.0 nM (95% CI=8.7~16.5 nM) while the Kd value of intact αPD-1 is 3.4 nM (95% CI=2,2~5.2 nM; Figure S2d), suggests αPD-1-ABD-PE has a weaker affinity to the EL4 cells than intact αPD-1.

We also incubated the labeled αPD-1-ABD-PE with the PD-1$^+$ and the PD-1$^-$ cells, separately, at 37°C (30 min) whereby both cell surface binding and cellular uptake were allowed to progress. After the incubation, the MFI of the PD-1$^+$ primary T cells, as measured by flow cytometry, was more than 8 times of that of PD-1$^-$ primary T cells (341.17 ± 31.97 versus 42.13 ± 2.00; Figure 1e); the MFI of the PD-1$^+$ primary B cells was more than 7 times of that of PD-1$^-$ primary B cells (321.17 ± 11.63 versus 41.98 ± 1.97; Figure 1f); the MFI of the EL4 cells after the incubation was approximately 12 times of that of the B16 cells (1532.70±4.99 versus 130.00±2.55; Figure S2e). In contrast, both the PD-1$^+$ and the PD-1$^-$ cells had low MFIs after incubation with labeled ABD-PE at 37°C (Figure 1e-f, Figure S2e). These data, together with the data generated at 4°C, suggest that αPD-1-ABD-PE specifically binds to and penetrates PD-1$^+$ cells and αPD-1 directs the specificity. PD-1 was found to shuttle its binding partners into cells and rapidly complete the transport, based on the fact that, 1) the MFI of EL4 cells after the 37°C incubation with αPD-1-ABD-PE was approximately several fold higher than the mean after the 4°C incubation, and 2) both incubations were only 30 minutes. It is worth noting that the same conclusion was reached using primary lymphocytes from both C57BL/6 (Figure 1 c-f) and NOD (Figure S2 f-i) mice.

We used an additional method to establish the role of PD-1 in the binding and internalization of αPD-1-ABD-PE to PD-1$^+$ cells. Here, we utilized a fusion protein of the ligand 1 of programmed death 1 protein and a human IgG Fc domain (PD-L1-Fc)[27] and performed a competitive binding assay (Figure 1g, Figure S3). We found concurrent incubation of αPD-1-ABD-PE and PD-L1-Fc with PD-1$^+$ cells abolished the binding and internalization of αPD-1-ABD-PE into PD-1$^+$ cells. Specifically, in the presence of PD-L1-Fc, the MFI of EL4 cells after the concurrent incubation at 4°C was approximately 8-time smaller than the MFI of the cells incubated with αPD-1-ABD-PE alone (74.58 ± 0.44 versus 583.80 ± 6.76, $P< 0.0001$; Figure 1g); and at 37°C, the MFI resulting from the concurrent incubation was decreased by approximately by 25 times as compared to that from the single incubation (74.52 ± 0.63 versus 1895.00 ± 34.82, $P< 0.0001$; Figure 1g). There data corroborate our studies presented above that the binding and internalization of αPD-1-ABD-PE into PD-1$^+$ cells were directed by PD-1. Interestingly, when EL4 cells were first incubated with αPD-1-ABD-PE at 37°C for 30 min and then with PD-L1-Fc added in the incubation mixture, PD-L1-Fc only partially decreased the MFI of the EL4 cells, from 1895.00 ± 34.82 to 1320.00 ± 120.30 (Figure 1g). The partial decrease may be because the PD-L1-Fc displaced surface bound αPD-1-ABD-PE but some αPD-1-ABD-PE has entered EL4 cells prior to the addition of PD-L1-Fc and, consequently, cannot be displaced by PD-L1-Fc. This observation is a proof that αPD-1-ABD-PE enter PD-1$^+$ cells. The conclusion about PD-1-mediated internalization is likely common to PD-1$^+$ cells of different types and origins, since results are consistent between PD-1$^+$ primary T and B cells and between cells collected from both C57BL/6 and NOD mice (Figure S3).

αPD-1-ABD-PE specifically depletes PD-1$^+$ cells both *in vitro* and *in vivo*

In vitro, αPD-1-ABD-PE was found to be at least hundred-time more lethal for PD-1$^+$ primary lymphocytes than for PD-1$^-$ primary lymphocytes: the IC_{50} of αPD-1-ABD-PE for PD-1$^+$ primary T cells was 0.43 nM (95% CI=0.27~0.69 nM) while αPD-1-ABD-PE did not

show detectable cytotoxicity to PD-1$^-$ primary T cells up to 100 nM (Figure 2a); the IC_{50} of αPD-1-ABD-PE for PD-1$^+$ primary B cells was 0.47 nM (95% CI=0.34~0.63 nM) while αPD-1-ABD-PE did not show toxicity to PD-1$^-$ primary B cells up to 100 nM (Figure 2b). A control mixture of αPD-1 and ABD-PE did not show cytotoxicity to either PD-1$^+$ or PD-1$^-$ primary lymphocytes up to 100 nm (Figure 2a-b). The hundred-times different toxicities between αPD-1-ABD-PE and the control mixture indicated the cytotoxicity of αPD-1-ABD-PE is due to a contiguous linkage between αPD-1 and ABD-PE. The same results were found in primary lymphocytes from both C57BL/6 (Figure 2a-b) and NOD mice (Figure S4a-b)

To pinpoint the role of αPD-1 in the selective cytotoxicity of αPD-1-ABD-PE to PD-1$^+$ cells, we generated a PD-1 knockout EL4 cell line (PD-1$^-$ EL4) using CRISPER/Cas9 (Figure S4c). We found that αPD-1-ABD-PE was more than 1000-time more toxic to wildtype EL4 cells than to PD-1$^-$ EL4 cells (IC_{50} = 0.64 nM 95% CI=0.49~0.83 nM versus IC_{50} = 1120 nM 95% CI=702.7~1773.0 nM; Figure 2c). By contrast, a control mixture of αPD-1 and ABD-PE had little or no cytotoxicity to both cell lines (IC_{50} = 590 nM 95% CI=458.7~760.6 nM for wildtype EL4 cells; IC_{50} = 1060 nM 95% CI=747.7~1514.0 nM for PD-1$^-$ EL4 cells). Together, these results point to a clear role of PD-1 in the PD-1+ cell selective toxicity of αPD-1-ABD-PE.

αPD-1-ABD-PE was also found to effectively deplete PD-1$^+$ cells *in vivo*. Specifically, a single dose of αPD-1-ABD-PE reduced the fraction of adoptively transferred EL4 cells to 2.86 ± 0.46% among circulating lymphocytes in the hosts; while mice treated with the mixture of αPD-1 and ABD-PE had unchanged EL4 cell fraction as compared to the PBS-treated mice (14.93 ± 1.36% versus 14.37 ± 1.60%; Figure 2d). The radically different cell depletion results between αPD-1-ABD-PE and the control mixture, again, confirm the importance of the linkage between αPD-1 and ABD-PE.

The ABD increases the plasma exposure of αPD-1-ABD-PE

We also examined the function of the ABD in αPD-1-ABD-PE. According to native PAGE results, there was a clear association of αPD-1-ABD-PE with mouse serum albumin (MSA, Figure 3a) and human serum albumin (HSA, Figure 3b). In contrast, αPD-1-PE did not associate with either MSA or HSA. These data suggest that the ABD component of αPD-1-ABD-PE retains its albumin-binding capacity and that the interaction between αPD-1-ABD-PE and albumin are due to the presence of the ABD. Next, we examined the pharmacokinetics of αPD-1-ABD-PE and αPD-1-PE after intraperitoneally dosing mice at 5.0 nmol per mouse (Figure 3c). Based on a non-compartmental analysis, αPD-1-ABD-PE has a systemic clearance (CL) that was approximately 30-fold less than that of αPD-1-PE (0.14 ± 0.01 mL/hr versus 4.05 ± 0.02 mL/hr), resulting in 30-time higher plasma exposure (area under curve, $AUC_{0\text{-}t}$); αPD-1-ABD-PE has a 57-fold longer terminal half-life ($t_{(1/2)}$) than αPD-1-PE (76.35 ± 9.13 hr versus 1.34 ± 0.02 hr). αPD-1-ABD-PE was also noted to be superior to αPD-1-PE in volume distribution (V_d) (Table 1). These data point to that the ABD in αPD-1-ABD-PE improved the PK of the construct, which was expected to benefit the efficacy of αPD-1-ABD-PE as poor PK was reported as an efficacy-limiting factor of previously developed immunotoxins[38].

αPD-1-ABD-PE delays the onset of T1D

Female non-obese diabetic (NOD) mice are prone to develop T1D[39]. We treated 12-week old female NOD mice that did not yet show hyperglycemia, with weekly injections of either, 1) αPD-1-ABD-PE, 2) PBS, or 3) a mixture of αPD-1 and ABD-PE. αPD-1-ABD-PE treatment markedly delayed the onset of T1D (hyperglycemia) as compared to PBS and the control mixture treatment. The median T1D-free survival time of the PBS-treated mice and the control mixture-treated mice were both 49 days after the treatment (P=0.3480 between the two treatments). In contrast, the median T1D-free survival time of the αPD-1-ABD-PE-treated mice was 119 days after the treatment (Figure 4a; P=0.0180 versus PBS treatment).

We also examined the delaying effect of αPD-1-ABD-PE in a pathologically accelerated T1D model. Ten-week old female NOD mice were pre-treated with cyclophosphamide (CP) to expedite the onset of T1D due to CP's ability to ablate regulatory T-cells (T_{REGS}) in NOD mice[40]. These CP pre-treated mice were subsequently treated with either 1) αPD-1-ABD-PE, 2) PBS, or 3) a mixture of αPD-1 and ABD-PE. Both the PBS-treated and the mixture control-treated mice had a very short median T1D-free survival of only 13 days. In contrast, the αPD-1-ABD-PE-treated mice had a significantly longer median T1D free survival, 33 days (Figure 4b; P=0.0068 versus PBS; P=0.0094 versus the mixture control). These data, taken together with the spontaneous T1D data, demonstrate that αPD-1-ABD-PE inhibits the development of T1D.

Since the pancreatic infiltrations of PD-1^+ cells and lymphocytes especially CD4+ lymphocyte parallel the progression of T1D in NOD mice[25, 39, 41], we investigated whether αPD-1-ABD-PE treatment would diminish the PD-1^+ cell and lymphocyte infiltrations (Figure S5). Indeed, even a single dose αPD-1-ABD-PE significantly reduced the fraction of PD-1^+ cells in pancreases as compared to PBS (0.17 ± 0.02 % versus 0.39 ± 0.03 %, P=0.0002; Figure 4c). In contrast, the control mixture did not reduce the fraction of PD-1^+ cells (0.56 ± 0.07 %, P=0.052). When these PD-1^+ cells were compared for the level of the PD-1 expression (MFI), the PD-1^+ cells survived the αPD-1-ABD-PE treatment had slightly but statistically significantly lower MFI (2132.17 ± 16.82, P=0.025) than the PD-1^+ cells survived the PBS treatment (2187.00 ± 12.12, Figure S6a). There was no significant difference between the cells of the PBS and the control mixture treatments. The result may be due to a preferential target of αPD-1-ABD-PE to PD-1^{high} cells over PD-1^{low} cells. Further, αPD-1-ABD-PE also significantly reduced the fractions of PD-1^+ CD4 T and PD-1^+ CD8 T cells in the pancreas as compared to PBS (P=0.0007 and 0.0002 respectively; Figure 4d-e). By contrast, the control mixture did not reduce the fractions of these two populations of PD-1^+ lymphocytes; the control mixture slightly increased the PD-1^+ CD4 T fraction. These fraction values also revealed that PD-1^+ CD4 T cells are the major PD-1^+ cells in the pancreases of the PBS treated mice; they account for approximately 75% of the PD-1^+ cells. There was no detectable population of PD-1^+ T_{REGS} or PD-1^+ B cells in the pancreases (Figure S6b-c). The αPD-1-ABD-PE treatment also reduced total CD4 and CD8 cells but not B cells in the pancreases, as compared to PBS (P=0.0002, 0.0008, and 0.119, respectively; Figure 4f-h). The mixture control, as expected, did not affect these cells. Thus, αPD-1-ABD-PE reduced the fractions of total PD-1^+ cells, PD-1^+ CD4 T cells, PD-1^+ CD8 T cells, CD4 T cells, and CD8 T cells in the pancreas of treated mice, which might

contribute to its marked delaying effect on T1D onset. Among these population, PD-1$^+$ CD4 T cells are likely a decisive factor given that they represent a major fraction of the PD-1$^+$ cells (75%) and their numbers were reduced by approximately 3 times after the αPD-1-ABD-PE treatment. We also attempted to examine PD-1$^+$ T cells and the PD-1$^+$ B cells in blood, spleens, and lymph nodes of these treated mice. However, these cells did not form distinguishable populations likely due to their scarcity (Figure S6d-i). In another word, the baseline numbers of PD-1$^+$ cells in blood and peripheral lymphatic organs are very low. Because of this result, it is expected that the total T and B cell numbers in these organs are not altered by αPD-1-ABD-PE treatments.

In addition to the pancreatic infiltration of lymphocytes, there was other data suggesting that αPD-1-ABD-PE selectively depletes autoreactive PD-1$^+$ cells in NOD mice (Figure 4i). Normally, αPD-1 accelerates T1D progression in NOD mice because it allows autoreactive PD-1$^+$ cells to proliferate[19, 24–27]. In this study, αPD-1 accelerated the onset of T1D in NOD mice that were pretreated with PBS and the mixture control: the median T1D-free survivals were 15 and 13 days, respectively (Figure 4i). In contrast, T1D exacerbating effect of αPD-1 diminished in αPD-1-ABD-PE pre-treated NOD mice: the mice did not show hyperglycemia even at the end of the experiment (26 days after the treatment). Because autoreactive PD-1$^+$ cells are primary effector cells that cause T1D and execute exacerbating effect of αPD-1, the diminished exacerbation effect of αPD-1 in the αPD-1-ABD-PE pre-treated mice suggests a reduction of autoreactive PD-1$^+$ cells in these mice.

αPD-1-ABD-PE treated mice recover from EAE

C57BL/6 mice immunized with $MOG_{35–55}$ in adjuvant develop a monophasic clinical disease where mice rarely recover[42, 43]. To test whether αPD-1-ABD-PE modulates EAE, C57BL/6 mice with EAE were treated with either, 1) αPD-1-ABD-PE, 2) PBS, or 3) a mixture of αPD-1 and ABD-PE. Before the treatment, all the mice had paralyzed hind limbs, a sign of severe EAE (clinical score 3.0). All six of the αPD-1-ABD-PE treated mice recovered from the paralytic diseases after a single dose (Figure 5a-b) and all had an EAE clinical score of 1.0 at the end of the study. In another replicate study, two of five αPD-1-ABD-PE treated mice had no clinical sign of EAE (fully recovered) at the end of this study (clinical score 0, Figure S7a). The other three mice in this replicate study had clinical scores of 1.0. In contrast, none of the paralyzed mice that received PBS or the mixture control treatment recovered. Instead, their EAE steadily worsened. The EAE scores of all mice in these two groups reached 4.00 by the end of this study. Indeed, from day 5 post treatment, the mean clinical score of the αPD-1-ABD-PE treated group was consistently and significantly lower than the scores of the PBS- and the mixture control-treated groups. It is noteworthy that mice in the three groups developed EAE with the same kinetics before the various treatments (Figure 5a): there was no significant difference in mean EAE scores among the three groups until day 19 after EAE induction ($P>0.05$ for all the monitored time points). At that time, some mice had received treatments, and the treatment had started to alter their EAE progression. The same EAE development kinetics among the three groups before the treatments, conversely, underscores the power of αPD-1-ABD-PE to interfere with and reverse the disease progression.

We investigated whether αPD-1-ABD-PE treatment reduced the infiltrations of PD-1$^+$ cells and lymphocytes into CNS of the mice with EAE. The presence of these cells especially CD4 cells in the CNS has been linked to EAE progression[18, 19, 44]. αPD-1-ABD-PE, even at a single dose, reduced the fraction of PD-1$^+$ cells in the CNS by more than 5 times as compared to PBS (Figure 5c; 0.19 ± 0.03 % versus 1.07 ± 0.09 %, P<0.0001). In contrast, the control mixture of αPD-1 and ABD-PE did not reduce the fraction of PD-1$^+$ cells in the CNS (1.19 ± 0.07 %, P=0.341). In regard of the PD-1 expression (MFI) of these PD-1$^+$ cells, the PD-1$^+$ cells collected from the αPD-1-ABD-PE treated mice had significantly lower MFI (1793.83 ± 11.55, P=0.0013) than the cells from the PBS treated mice (1877.83 ± 15.2, Figure S7b). Interestingly, the cells collected from the control mixture treated mice had slightly lower MFI (1836.00 ± 8.14) as well. Further, αPD-1-ABD-PE significantly reduced the fractions of PD-1$^+$ CD4 T, and PD-1$^+$ CD8 T cells in the CNS as compared to PBS (P<0.0001 and P=0.003 respectively; Figure 5d-e). In contrast, the control mixture did not reduce the fractions of these PD-1$^+$ lymphocytes in the CNS. PD-1$^+$ CD4 T cells account for the vast majority of PD-1$^+$ cells in the CNS of the mice with EAE (98.1% in the PBS treated mice). There was no detectable population of PD-1$^+$ Tregs or PD-1$^+$ B cells in the CNS (Figure S7c-d). The αPD-1-ABD-PE treatment also reduced total CD4 T and CD8 T cells but not B cells in the CNS, as compared to PBS (P<0.0001, P=0.0001, and P=0.567 respectively; Figure 5f-h). The mixture control, as expected, did not affect these cells. Lastly, we compared the ratios between Tregs and MOG peptide-specific CD4 T cells ($MOG_{38–49}$: GWYRPPFSRVVH) in the CNS among the three treatments. This MOG-specific clone is the main autoreactive T effector cell clone in this EAE model[45]. We found the αPD-1-ABD-PE treatment boosted the ratio by approximately 4 times, as compared to PBS (P<0.0001, Figure 5i). The increased ratio was due to that Treg fraction in the CNS was not changed after the αPD-1-ABD-PE treatment (Figure S7e) but the MOG-specific CD4 T cells decreased (Figure S7f). The mixture control did not significantly alter the ratio (Figure 5i). Taken together, these results suggest that the αPD-1-ABD-PE treatment diminished the infiltrations of PD-1$^+$ cells and T cells into the CNS of treated mice and the treatment increase the Treg-to-effector cell ratio, a sign favoring immune tolerance.

We also examined PD-1$^+$ T cells and the PD-1$^+$ B cells in blood, spleens, and lymph nodes of treated mice, same as what we conducted in NOD mice. However, we did not discern these populations (Figure S7g-l).

αPD-1-ABD-PE does not compromise normal adaptive immune responses

The αPD-1-ABD-PE treatment did not cause lymphopenia that is often associated with therapeutics for autoimmune diseases[6, 9–12, 46]. We compared the B220+, CD4+ and CD8+ lymphocytes in blood and spleens of C57BL/6 mice (Figure 6a) after mice received one dose of 1) αPD-1-ABD-PE, 2) PBS, 3) a mixture of αPD-1 and ABD-PE, or 4) cyclophosphamide (CP). CP is a non-specific immunosuppressant used here as a positive control for immune suppression. αPD-1-ABD-PE did not reduce the numbers of these three lymphocyte sub-populations as compared to the PBS treatment (Figure 6a-b). Similarly, the mixture control did not affect the proportions of these lymphocyte sub-populations. However, CP reduced the numbers of B220+, CD4+ and CD8+ lymphocytes in blood averagely by 70.1%, 69.5%, and 75.6%, respectively (P<0.0001, P=0.0002, and P=0.0002,

respectively; Figure 6a); CP reduced the numbers of B220+, CD4+ and CD8+ lymphocytes in spleens by 46.0%, 76.0%, and 70.1%, respectively (P=0.0002, P<0.0001 and P<0.0001, respectively; Figure 6b). These findings were reproducible in NOD mice (Figure S8a-b).

The αPD-1-ABD-PE treatment did not affect antibody responses in treated mice. Here, we first treated C57BL/6 and NOD and mice with one dose of 1) αPD-1-ABD-PE, 2) PBS, 3) a mixture of αPD-1 and ABD-PE, or 4) CP. Two days later, these mice were immunized with DNP-Ficoll, a T cell-independent antigen[47]. We found that both the αPD-1-ABD-PE-treated mice and the mixture control-treated mice developed the same level of anti-DNP responses as the PBS-treated mice (Figure 6b, Figure S8c-f). However, CP-treated mice developed weaker anti-DNP responses. These findings were reproduced in both C57BL/6 and NOD mice. It is noteworthy that the same conclusion was reached in mice that were treated with five-doses of αPD-1-ABD-PE and its controls (Figure S8g-h).

The αPD-1-ABD-PE treatment did not affect cytotoxic T lymphocyte (CTL) responses. Here, we first treated C57BL/6 and NOD mice with one dose of 1) αPD-1-ABD-PE, 2) PBS, or 3) a mixture of αPD-1 and ABD-PE, or 4) CP. Two days after the dosing, treated NOD mice were immunized with TYQRTRALV, a CTL epitope vaccine that matched with the MHC class I background of NOD mice; whereas, treated C57BL/6 mice were immunized with SIINFEKL, a CTL vaccine that was derived from ovalbumin (residues 257–264) and matched with the MHC class I background of C57BL/6 mice. We observed that the αPD-1-ABD-PE-treated mice, the mixture control-treated mice and the PBS-treated mice all developed the same degree of CTL responses (Figure 6c). In contrast, the CP-treated mice developed weaker CTL responses as compared to the PBS treated mice (p= 0.011 and 0.026 for C57BL/6 and NOD mice, respectively). These findings were noted in both C57BL/6 and NOD mice.

These data, together, showed that αPD-1-ABD-PE treatment did not significantly alter the ability of the treated mice to mount antibody and/or CTL responses.

Discussion:

According to results of this study, αPD-1-ABD-PE has specific toxicity to PD-1$^+$ B and T cells; PD-1$^+$ cell depletion, enabled by αPD-1-ABD-PE, ameliorates autoimmunity in multiple disease models that are different in pathogenesis; and application of PD-1$^+$ cell depletion does not cause adaptive immune deficiency.

PD-1$^+$ cell depletion effectively ameliorated disorders in several autoimmune disease models. In a chronic EAE model, even a single dose of αPD-1-ABD-PE fully restored mobility in mice that were paralyzed by EAE, which is a rarely achieved therapeutic outcome. In addition, the single dose of αPD-1-ABD-PE significantly reduced PD-1$^+$ cell, T lymphocytes, and autoreactive lymphocytes in CNS of the treated mice. Current therapies for MS are termed disease-modifying therapies because they only delay disease progression and do not reverse or cure the disease[6, 11]. The noted efficacy of PD-1$^+$ cell depletion may render the depletion able to fill a significant clinical gap in MS treatment. In regard of T1D, PD-1$^+$ cell depletion markedly delayed T1D onset in a spontaneous model as well as in two

accelerated T1D models (CP treatment and αPD-1 IgG treatment). Under the conditions studied, T1D eventually developed in the spontaneous and the CP-accelerated models after significant delays. Nevertheless, it is possible that the efficacy of PD-1$^+$ cell depletion will be further boosted by regimens that are optimized with the pharmacokinetics-pharmacodynamics of αPD-1-ABD-PE. The improved efficacy may allow the depletion to completely prevent T1D. This possibility is supported by the observed broad impact of a single dose of αPD-1-ABD-PE on immune cells in pancreases; the dose decreases the fractions of PD-1$^+$ CD4 T cells, PD-1$^+$ CD8 T cells, as well as total CD4 and CD8 T cells, a global attenuation of the inflammation in pancreases. PD-1$^+$ cell depletion may also be helpful to reverse T1D in combination with β-cell compensation therapy[2, 4]. It is noteworthy that PD-1$^+$ cell depletion delayed the onset of CP-induced T1D. First, the observation implies that PD-1$^+$ cells may be the primary effector cells in autoimmunity driven by Treg deficiency since CP causes Treg deficiency[40]. Second, the observation suggests that the depletion may be able to resolve the autoimmunity that does not originate from the abnormality of the PD-1 checkpoint. Together, PD-1$^+$ cell depletion is efficacious in EAE and T1D, the two T cell-driven autoimmune disease models; PD-1$^+$ CD4 T cells appeared to be the major pathogenic cell population in the two models and responded well to PD-1$^+$ cell depletion.

PD-1$^+$ cell depletion will likely be effective to B-cell mediated autoimmune diseases. First, these autoimmune diseases like SLE depend on not only B cells but also CD4 T cells such as Tfh and extrafollicular Th. These CD4 T cells facilitate the formation of germinal center, the maturation of B cells, and antibody production[48]. Meanwhile, our results show PD-1$^+$ cell depletion diminished both PD-1+ CD4 T cells and total CD4 T cells (Figures 4-5). Further, our results confirmed that αPD-1-ABD-PE is able to specifically bind to, penetrate, and eliminate PD-1$^+$ primary B cells. Last, PD-1 knockout mice have elevated IgG production and eventually assume lupus-like symptoms[48]. One interpretation for this observation is that activated autoreactive cells in the mice escape the PD-1 immune checkpoint and cause the lupus-like symptoms since these cells do not express PD-1. In contrast, activated autoreactive cells are PD-1-positive in wildtype mice and hence inhibited by the checkpoint. In mice with SLE, the checkpoint fails to suppress activated autoreactive cells. However, it is possible to utilize PD-1 as a biomarker to identify and deplete the cells and assuage autoimmune destruction in the mice with SLE. Taken together, PD-1$^+$ cell depletion impacts both PD-1$^+$ B and CD4 T cells and likely alleviate B-cell mediated autoimmune diseases.

PD-1$^+$ cell depletion preserves normal adaptive immunity, which sharply contrasts from the generalized immune deficiency caused by currently available immune suppressants[6, 9–12, 46]. It is acknowledged that PD-1$^+$ cell depletion could diminish non-autoreactive PD-1$^+$ lymphocytes including PD-1$^+$ effector cells and Tregs[49]. However, we feel this only represents a theoretical concern. First, PD-1$^+$ effector cells can be replenished from naïve lymphocytes upon immune stimulation as lymphocyte repertoires are not impaired by PD-1$^+$ cell depletion. Second, PD-1$^+$ cells are scarce and hardly detectable in blood and peripheral lymphatic organs in mice with T1D and EAE, rather they are relatively concentrated in inflamed organs (Figures 4-5, Figures S6–7). This intrinsic distribution of PD-1$^+$ cells helps to alleviate the negative impact of PD-1$^+$ cell depletion on non-autoreactive lymphocytes. Last, the finding that PD-1$^+$ cell depletion preserves adaptive immunity argues against the

theoretical concern; mice experienced the depletion were able to mount normal immune responses as soon as two days after the depletion. There is additional rational supporting the depletion of PD-1$^+$ cells in autoimmune diseases including non-autoreactive PD-1$^+$ cells. In the context of autoimmune diseases, the immune system is, overall, tilted toward autoimmunity rather than immune tolerance or anergy[50]. Autoreactive, PD-1$^+$ lymphocytes outweigh their non-autoreactive counterparts including PD-1$^+$ Tregs[49] in terms of impact to the well-being of patients. Thus, it is arguably beneficial to purge all PD-1$^+$ cells, reprogram the immune system, and restore immune homeostasis. PD-1$^+$ cell depletion, indeed, resembles systemic γ-irradiation or lymphocyte depletion that have both been used to reprogram the immune system[51]. Yet, PD-1$^+$ cell depletion is a much more focused approach than these reported approaches. One observation that supports this idea of purging PD-1$^+$ cells is that the αPD-1-ABD-PE treatment, while reducing PD-1$^+$ CD4 T cells, PD-1$^+$ CD8 T cells, and autoreactive T cells in pancreases of NOD mice as well as the CNS of the mice with EAE, did not diminish Tregs in these organs. Indeed, the depletion increased the ratios between Treg and autoreactive cells in the CNS, which favors the treatment of autoimmune diseases.

Targeted depletion of PD-1$^+$ cells, enabled by αPD-1-ABD-PE, has shown three appealing features as a new therapeutic option for autoimmune diseases. First, the depletion has a straightforward and robust working mechanism. It relies on a simple cytotoxic mechanism to kill PD-1$^+$ cells; yet, a single administration of depletion can suppress autoimmunity completely such as enabling paralyzed mice to regain normal gait. Second, the depletion is capable to suppress both the T and B cell mediated autoimmunity in one autoimmune disease. It also has potential to treat primarily T cell- or B cell-driven autoimmune diseases. Last, the depletion does not cause long-term immune deficiency. Although the depletion can deplete non-autoreactive PD-1$^+$ cells and may affect the healthy immunity at the moment of the action, the immunity appears to recover very quickly because of preservation of naive cells. Indeed, as soon as two days after the depletion, the αPD-1-ABD-PE treated mice were able to mount the same strength of adaptive responses as the PBS treated mice. Thus, the depletion did not impact healthy immunity for long-term. In summary, targeted depletion of PD-1$^+$ cells is an effective and broadly applicable approach to treat autoimmune diseases without jeopardizing healthy immunity.

METHODS:

Animal and cell lines

Female C57BL/6 mice were purchased from The Jackson Laboratories. Female NOD mice were purchased from The Jackson Laboratories and bred in-house. Animal studies were conducted following a protocol approved by the Institutional Animal Care and Use Committee (IACUC) at the University of Utah. The group sizes of mice were determined and approved by the regulatory authorities for animal welfare after a balanced consideration of statistical and scientific needs and ethical aspects. All procedures related to animal studies are in compliance with relevant ethical regulations on animal research at the University of Utah. The EL4 and B16-F10 (abbreviated as B16 cells) cell lines were purchased from the ATCC and maintained in DMEM medium with 10% FBS.

Antibodies

Capture anti-mouse IFN-γ mAb (clone: R4–6A2) and biotinylated, detection anti-mouse IFN-γ mAb (clone: XMG1.2-Biotin) were purchased from BioLegend, San Diego, CA. Peroxidase-conjugated AffiniPure Donkey Anti-Mouse lgM and Peroxidase AffiniPure Goat Anti-Mouse IgG (H+L) were purchased from Jackson ImmunoResearch Inc. Anti-mouse CD-3 antibody (clone: 145–2C11) was purchased from BioXCell, West Lebanon, NH. FITC-, PE-, APC- or biotin-conjugated monoclonal antibodies to Foxp3 (clone: MF-14), B220 (clone: RA3–6B2), CD4 (clone: GK1.5), and CD8 (clone: 53–6.7) were purchased from BioLegend, San Diego, CA.

Generation of expression vectors for recombinant proteins

Genes encoding αPD-1 (scFv), PE, or ABD-PE were synthesized by Biomatik. All the genes were inserted into the pET25b (+) vector at the BseRI restriction sites. The configuration of the αPD-1 (scFv) was NH_2-V_H-Linker-V_L-COOH where V_H and V_L were the variable regions of the αPD-1 heavy chain and the αPD-1 light chain, respectively. Two mutations were introduced in the αPD-1, V_H: R45C; V_L:G104C. The linker inside the αPD-1 was $(GGGGS)_3$. The linker was also inserted in between the ABD domain and the PE domain of ABD-PE. The coding genes of αPD-1-ABD-PE and αPD-1-PE were generated by fusing the synthesized genes together using a previously described protocol [52, 53]. Meanwhile, a gene that encodes the linker was inserted between the genes of αPD-1 and ABD-PE, and between the genes of αPD-1 and PE. The linker gene was generated by annealing the sense and antisense oligonucleotides of the gene (Eurofins Genomics). A hexa-histidine tag (HisTag) was added at the NH_2-terminus of αPD-1-ABD-PE and its control proteins to facilitate the purification of these proteins; a linker, GGGGS, was inserted between the HisTag and the proteins. Accordingly, the coding gene of the HisTag was also fused to the coding genes of these proteins. The lengths of the finally resultant genes were confirmed by agarose gel electrophoresis after they were cleaved from pET25b (+) vector by double digestion with BamHI and XbaI. The sequences of these genes were verified by DNA sequencing (Genewiz).

Protein expression and purification

The pET25b (+) vectors that harbor coding genes of αPD-1-ABD-PE, αPD-1, ABD-PE, and αPD-1-PE were transferred into competent Shuffle T7 *E. coli* cells (New England Biolabs). These transformed *E. coli* cells were cultured in LB broth at 32 °C until the optical density (OD_{595}) of the culture reached 0.6. At that point, the cultured cells were induced with 1 mM final concentration IPTG (Gold Biotechnology) for protein expressions that lasted 18 hours.

The cultured *E. coli* cells were harvested by centrifuging the culture at 4,700 rpm for 30 minutes. The collected cells were lysed by sonication using the 4-minute ON time. The cell samples were kept on ice during sonication, and 1 mM PMSF (Gold Biotechnology) was added to the cell lysate to inhibit protein degradation. After sonication, the supernatant of the cell lysate was collected by centrifuging the lysed samples at 20,000 g for 1 hour. Next, imidazole powder was added into the supernatant to reach a final imidazole concentration of 20 mM. At the same time, HisPur Ni-NTA resin (Thermo Fisher Scientific) was equilibrated with 10 mM imidazole in PBS. The equilibrated resin was then incubated with the

supernatant for 1 hour at 4 °C on a rotator mixer. After the incubation, the mixture was loaded on a column, and the impurities and endotoxins were removed by washing the column with 60 mM imidazole that contained 1% Triton X-114. The wash was repeated until protein concentrations in the eluent were very low ($OD_{280} < 0.01$). The method to use 1% Triton X-114 for endotoxin removal was described previously [54]. After this purification step, Triton X-114 was removed by washing the column with 50 column volumes of 60 mM imidazole. Finally, the desired proteins were eluted from the column with 300 mM imidazole in PBS (pH=8). Imidazole was removed by PD-10 desalting columns (GE Healthcare Life Sciences). The purity and residual endotoxin level of the product proteins were analyzed by SDS-PAGE and PYROGENT single test vials (Lonza, Allendale, NJ).

SDS-PAGE analysis of proteins

5 μg of αPD-1, ABD-PE, αPD-1-PE, and αPD-1-ABD-PE were first reduced by 2-Mercaptoethanol and denatured by heating the samples at 95 °C for 5 minutes. Then, these denatured samples were analyzed on a 4–15% gradient SDS-PAGE gel. After the electrophoresis, the gel was stained with Coomassie brilliant blue and photographed using an Alpha Innotech Fluorchem FC2 gel imaging system. The picture was processed by adjusting the brightness and contrast for the entire images. An open-source software GNU Image Manipulation Program (GIMP) was used to process the image.

Determination of the binding affinity of αPD-1-ABD-PE to EL4 cells

1 million of EL4 cells were incubated with Alexa Fluor 647-labeled αPD-1-ABD-PE and αPD-1 IgG at a series of different concentrations of 4 °C for 30 min. Then, the EL4 cells were analyzed by flow cytometry for $PD\text{-}1^+$ fractions of EL4 cells. $PD\text{-}1^+$ fraction of EL4 cells were plotted against protein concentrations and K_d values were obtained by fitting the curve using sigmoidal dose-response model in GraphPad V5. EC_{50} values were used as the K_d values [55]. 95% confidential intervals (95% CI) were calculated by GraphPad.

Generation of $PD\text{-}1^+$ primary T cells

Mouse splenocytes were harvested and cultured in 96-well plates at 2×10^6 /mL in complete RPMI-1640. Then, concanavalin A (Con A) (InvivoGen) was added into the cutlture at 6.25 μg/mL to stimulate PD-1 expression on primary T cells [14]. After 72-hour stimulation, cells were collected. $PD\text{-}1^-$ primary T cells were naïve splenocytes cultured in complete RPMI-1640 without Con A for 72 hours. These primary T cells were stained with αCD3-PE during later flow cytometry analysis.

Generation of $PD\text{-}1^+$ primary B cells

Mouse splenocytes were harvested and cultured in 96-well plates at 2×10^6 /mL in complete RPMI-1640. Then, 10 μg/mL AffiniPure $F(ab')_2$ fragment of goat anti-mouse IgM, μ Chain Specific (Jackson ImmunoResearch, code 115–006-020) was added into culture to stimulate PD-1 expression on primary B cells [14]. After 72-hour stimulation, the cells were collected. $PD\text{-}1^-$ primary B cells were naïve splenocytes cultured in complete RPMI-1640 without anti-IgM for 72 hours. These primary B cells were stained with αB220-PE during later flow cytometry analysis.

Evaluation of cell binding and endocytosis

αPD-1-ABD-PE or ABD-PE were first labeled with Alexa Fluor 647 NHS Ester (Thermo Fisher Scientific). The labeled αPD-1-ABD-PE or ABD-PE (100 nM) were incubated with 0.5 million of cells separately. The incubation mixtures were maintained at 4 °C or 37 °C in FACS buffer (PBS with 0.1% FBS) for 30 minutes. After the incubation, unbound proteins were removed by centrifugation (350 g for 5 minutes). Last, the median fluorescence intensity (MFI) of these incubation mixtures were determined by flow cytometry with a BD FACSCanto Analyzer (BD Biosciences).

Specifically, for primary B cells, the MFI values of B-cell populations were analyzed. B-cell populations were identified by staining the cell mixture by αB220-PE.

For primary T cells, the MFI values of T-cell populations were analyzed. T-cell populations were identified by staining the cell mixture by αCD3-PE.

Binding inhibition study with PD-L1-Fc

A PD-L1-Fc was used to compete surface PD-1 binding of αPD-1-ABD-PE. The PD-L1-Fc is a fusion protein between mouse PD-L1 and human Fc, Sino Biological, 50010-M03H). For concurrent incubation, the PD-L1-Fc was added to a final concentration of 500 nM with Alexa Fluor 647-labeled αPD-1-ABD-PE (100 nM final concentration) into 0.5 million cells and incubated for 30 min at 4 °C or 37 °C. Then, unbound proteins were washed away by centrifugation (350 g for 5 minutes) in FACS buffer. The cells were analyzed by flow cytometry with a BD FACSCanto Analyzer (BD Biosciences). Human IgG at 500 nM was used as the control for PD-L1-Fc fusion.

In the experiment surface-bound αPD-1-ABD-PE is need to be stripped, Alexa Fluor 647-labeled αPD-1-ABD-PE was first incubated with 0.5 million of cells for 30 min at 37 °C, then PD-L1-Fc was added to a final concentration of 500 nM. The incubation mixtures were kept at 4 °C for additional 30 min before unbound proteins were washed away by centrifugation (350 g for 5 minutes) in FACS buffer. The cells were analyzed by flow cytometry with a BD FACSCanto Analyzer (BD Biosciences).

Generation of PD-1^{-} EL4 cell line

We chose a single guide RNA (sgRNA) sequence in the exon 2 of the mouse PD-1 gene Pdcd1 (NC_000067.6) based on an algorism described previously [56]. The sequence of sgRNA was *CCTTGACACACGGCGCAATGACAGTGGCAT*. The protospacer adjacent motif (PAM) was *TGG*. To target this sgRNA, two oligos were commercially synthesized (Integrated DNA Technologies): 5'- *CACCGGACACACGGCGCAATGACAG* −3' and 5'- *AAACCTGTCATTGCGCCGTGTGTCC* −3'. The two oligos were annealed and ligated into the lentiviral vector lentiCRISPRv2-mCherry, which was kindly provided by Dr. Vicente Planelles (University of Utah). High-title lentiviral supernatants were generated as previously described [57] by co-transfection of HEK293T cells (ATCC) with the packaging plasmids pMD2.G (Addgene 12259) and psPAX2 (Addgene 12260). After EL4 cells were transduced with lentiviral supernatants, the transductants were stained with PE-Cy7 conjugated anti-PD-1 antibody (BioLegend, Clone: RMPI-30) and sorted for mCherry

$^{+}$PD-1^{-} cells with FACSAria™ cell sorter (BD Biosciences) at the Flow Cytometry Core of the University of Utah. The EL4 and 293T cell lines were maintained in DMEM with 10% FBS.

Cytotoxicity study

For the cytotoxicity study with PD-1^{+} primary T cells, naïve splenocytes (concentration 2×10^{6} /mL) were first stimulated with 6.25 μg/mL Con A for 24 hours. Then, αPD-1-ABD-PE or the control mixture were added into the wells without removing Con A. 2 days after adding drugs, cells were harvested. Live cells were counted after stained with trypan blue. The percentage of PD-1^{+} primary T cells among these live cells were determined by flow cytometry after the live cells were stained with αCD3-PE (Biolegend), 3 μM DAPI (4',6-Diamidino-2-Phenylindole, Dilactate) (Biolegend), and αPD-1-Alexa Fluor 647 that was made in house. Last, the number of live PD-1^{+} primary T cells were calculated by multiplying the number of total live cells and the percentage of PD-1^{+} primary T cells. For cytotoxicity study PD-1^{-} primary T cells, naïve splenocytes (concentration 2×10^{6} /mL) were first culture in complete RPMI-1640 for 24 hours. Then, αPD-1-ABD-PE or the control mixture were added in the culture. Two days later, cells were harvested and analyzed same as described above. The total number of live cells, the percentage of PD-1^{-} primary T cells, as well as the number of live PD-1^{-} primary T cells were determined in the same way as that of PD-1^{+} primary T cells.

The cell viabilities were calculated for different concentrations of αPD-1-ABD-PE and the control mixture using the following equation. The viability data was fitted to a Sigmoidal dose-response model to determine IC_{50} and 95% CI using GraphPad V5 (N = 6).

The equation for cell viability:

$$\text{Cell viability}(\%) = [\text{PD-1}^{+}\text{ (or PD-1}^{-}\text{) T cell number of treated well}] / [\text{PD-1}^{+}\text{(or PD-1}^{-}\text{) T cell number of untreated well}].$$

The toxicity study with PD-1^{+} and PD-1^{-} primary B cells was the same as the one with T cells except that anti-mouse IgM was used to stimulate B cells and αB220-PE was used to stain B cells.

For cytotoxic studies on EL4 cells and PD-1^{-} EL4 cells, EL4 cells or PD-1^{-} EL4 cells (10,000 cells/well) were seeded into 96-well plates. αPD-1-ABD-PE or control mixture were incubated with the cells in 100 μL medium at 37 °C for 72 hours. After the incubation, proliferations of these cell samples were determined by the CellTiter MTS assay (Promega), and the OD_{490} of each treated cell sample was measured. The same measurement was also conducted for untreated cells (the live control) and the cells that were treated with 1% Triton X-100 (the dead control). These control cell samples were also cultured for 72 hours and their proliferations were determined the same as αPD-1-ABD-PE-treated cells. The cell viabilities were calculated for different concentrations of αPD-1-ABD-PE and the control mixture using the following equation. The viability data was fitted to a Sigmoidal dose-response model to determine IC_{50} and 95% CI using GraphPad V5 (N = 6).

The equation for cell viability:

$$\text{Cell viability}(\%) = (OD_{\text{treated}} - OD_{\text{dead control}}) / (OD_{\text{live control}} - OD_{\text{dead control}}).$$

OD_{treated}: OD_{490} of the αPD-1-ABD-PE or the control treated cells,

$OD_{\text{live control}}$: OD_{490} of the live control,

$OD_{\text{dead control}}$: OD_{490} of the dead control (Triton X-100 treated cells)

In vivo EL4 depletion

Five million of EL4 (PD-1-positive) cells were injected into C57BL/6 mice intravenously through their tail veins. The injected mice were randomly assigned into 3 groups. Two hours later, the three groups were treated with a single dose of αPD-1-ABD-PE (5 mg/kg), a mixture of αPD-1 (scFv, 2.5 mg/kg) and ABD-PE (2.5 mg/kg), or PBS intraperitoneally. At 72 hours after the treatments, these mice were euthanized, and circulating lymphocytes were collected from the mice. The cells were stained with Alexa Fluor 647-labeled αPD-1 and analyzed by flow cytometry with a BD FACSCanto Analyzer. The fractions of PD-1-positive cells among circulating lymphocytes were determined through the analysis.

Albumin-binding study

MSA (>96% pure, Sigma) and HSA (>97% pure, Sigma) were dissolved in PBS. 17.4 μg of αPD-1-ABD-PE or 15.9 μg of αPD-1-PE were incubated with 20.0 μg MSA (1:1 molar ratio) in 20 μL PBS at room temperature for 15 minutes. After incubation, the samples were analyzed by native PAGE. The PAGE gel was stained by Coomassie brilliant blue and photographed using an Alpha Innotech Fluorchem FC2 gel imaging system. The picture was processed by adjusting the brightness and contrast for the entire images. An open-source software GNU Image Manipulation Program (GIMP) was used to process the image.

Regarding HSA, the amount of proteins used is the same as MSA incubation experiment. After incubation, the samples were analyzed as described above.

Pharmacokinetics (PK)

Five nmole of αPD-1-ABD-PE or αPD-1-PE that were labeled by NHS-Fluorescein (Thermo Fisher Scientific Inc) were injected intraperitoneally into C57BL/6 mice. At each pre-determined time point (0.25, 1, 2, 4, 8, 12, 24, and 48 hours after dosing), a cohort of three mice was sacrificed, and the blood were collected for quantification of protein concentration. Plasma concentrations of the proteins were determined according to the fluorescence intensity (Ex 494 nm /Em 518 nm). The pharmacokinetics of both proteins was analyzed using non-compartmental analysis (Phoenix WinNolin software, version 8.0, Pharsight Corporation, CA, USA) [58]. PK parameters CL, $t_{1/2}$, $AUC_{0\text{-}t}$, and V_d were calculated.

Disease delay study with a spontaneous T1D model

Twelve-week-old female NOD mice were randomly assigned into three groups. The three groups were treated intraperitoneally with αPD-1-ABD-PE (5 mg/kg), a mixture of αPD-1

(scFv, 2.5 mg/kg) and ABD-PE (2.5 mg/kg), or PBS weekly until the mice were found to be diabetic. Blood glucose levels of these mice were monitored twice weekly using a OneTouch UltraMini Blood Glucose Meter (LifeScan, Inc). The T1D onset was confirmed for a mouse when blood glucose concentrations of the mouse were greater than 250 mg/dL in two consecutive measurements. Diabetes-free survival was analyzed by the Kaplan-Meier method followed the Log-rank (Mantel-Cox) test using GraphPad Prism V5.

Disease delay study with a cyclophosphamide (CP)-accelerated T1D model

Ten-week-old female NOD mice were injected intraperitoneally with CP (Santa Cruz Biotechnology) at 200 mg/kg. Two days later, these mice were randomly assigned into three groups. The three groups were treated intraperitoneally with αPD-1-ABD-PE (5 mg/kg), a mixture of αPD-1 (scFv, 2.5 mg/kg) and ABD-PE (2.5 mg/kg), or PBS every other day for a total of five treatments. The diabetes-free survival data were generated and analyzed as described above.

Disease delay study with a αPD-1-accelerated T1D model

Ten-week-old female NOD mice were randomly assigned into three groups. The three groups were treated intraperitoneally with αPD-1-ABD-PE (5 mg/kg), a mixture of αPD-1 (scFv, 2.5 mg/kg) and ABD-PE (2.5 mg/kg), or PBS every other day for totally five treatments. Two days after the last dosing, 0.5 mg/mouse αPD-1 IgG (clone RMP1–14)[59]) was administered intraperitoneally to all the mice. Two days later, all these mice received four additional doses of αPD-1 IgG with a two-day interval at a dose level of 0.25 mg/mouse/injection. The diabetes-free survival data were collected and analyzed as described above.

Examination of immune cells in pancreases, blood, and peripheral lymphatic organs of pre-diabetic NOD mice

Eighteen-week-old, prediabetic, female NOD mice were randomly assigned into three groups. The three groups were treated intraperitoneally with one dose of αPD-1-ABD-PE (5 mg/kg), a mixture of αPD-1 scFv (2.5 mg/kg) and ABD-PE (2.5 mg/kg) or PBS. Three days later, these mice were euthanized and perfused with 30 mL PBS. Pancreases were collected from these mice and a single cell preparation was generated from each of the pancreases by mincing the pancreas tissues with scissors and digesting the tissues with 1 mg/mL collagenase IV at 37 °C for 30 minutes as described previously [60]. The pancreatic cell preparations were filtered through a nylon mesh and then dead cells were first stained by 3 μM DAPI for 10 min, and then washed 3 times by a centrifugation (300 g for 5 minutes) to remove DAPI. Cells were then stained with αB220-PE, αCD8-PE, αCD3-PECy7, αCD4-FITC, αFOXP3-PE (all antibodies were purchased from Biolegend), and αPD-1-Alexa Fluor 647 that was made in house. Lastly, 400,000 live cells per pancreatic cell preparation were analyzed by flow cytometry with a BD FACSCanto Analyzer.

To analyze immune cells in blood and peripheral lymphatic organs, blood, spleens, lymph nodes (accessory axillary lymph nodes and subiliac lymph nodes) were collected from the aforementioned mice. Red blood cells in these samples were lysed with the Ammonium-Chloride-Potassium (ACK) Lysing Buffer. The remaining cells were pelleted by a

centrifugation at 300 g for 5 minutes, and stained by DAPI (3 μM), αB220-PE, αCD8-PE, αCD4-PECy7, αCD3-FITC, αFOXP3-PE, and αPD-1-Alexa Fluor 647 that was made in house. Lastly, 10,000 live cells per cell preparation were analyzed by flow cytometry with a BD FACSCanto Analyzer.

Disease reversal study in an EAE model

Ten-week-old female C57BL/6 mice were subcutaneously immunized with 0.2 mg $MOG_{35–55}$ peptide (MEVGWYRSPFSRVVHLYRNGK, Biomatik) per mouse. The peptide was emulsified in 0.2 mL CFA (Sigma). Four hours later, all mice received intraperitoneally 200 ng pertussis toxin (List Biological Labs, Inc). And 24 hours later, all mice received an additional 200 ng pertussis toxin. The immunized mice were examined for their paralysis symptoms every other day from the 9th day after the immunization. The symptoms were scored based on a common standard [61]: 1.0, limp tail or isolated weakness of gait without limp tail; 2.0, partial hind leg paralysis; 3.0, total hind leg or partial hind and front leg paralysis; 4.0, total hind leg and partial front leg paralysis; 5.0, moribund or dead animal. At the same time, the immunized mice were randomly assigned into three groups; each group would receive one of the three treatments: αPD-1-ABD-PE (5 mg/kg), a mixture of αPD-1 (scFv, 2.5 mg/kg) and ABD-PE (2.5 mg/kg), or PBS. When an immunized mouse developed severe EAE (clinical score 3.0), this mouse would be immediately treated according to its group assignment. All the treated mice were continuously monitored until they reached their humane endpoints or the end of the study.

Examination of immune cells in pancreases, blood, and peripheral lymphatic organs of mice with EAE

Ten-week-old female C57BL/6 mice were induced for EAE as described above. After all induced mice developed severe EAE (clinical score 3.0), the mice were randomly assigned into three groups that received αPD-1-ABD-PE (5 mg/kg), a mixture of αPD-1 (scFv, 2.5 mg/kg) and ABD-PE (2.5 mg/kg), or PBS intraperitoneally. Three days later, these mice were euthanized and perfused with 30 mL PBS after blood was collected. The spinal cord and brain were collected from these mice, and were subsequently minced digested as described above. A single cell preparation was generated by filtering the processed tissues of one mouse through a nylon mesh. Mononuclear cells were enriched in the preparations by passing the preparations through a discontinuous 30%:70% Percoll gradient as described previously [62, 63]. The resultant cell preparations were stained and analyzed by flow cytometry. Dead cells were first stained by 3 μM DAPI for 10 min, and then washed 3 times by a centrifugation (300 g for 5 minutes) to remove DAPI. Then cells were stained with αB220-PE, αCD8-PE, αCD3-PECy7, αCD4-FITC, αFOXP3-PE (all antibodies were purchased from Biolegend), I-A^b $MOG_{38–49}$-PE tetramer (provided by NIH tetramer care facility), and αPD-1-Alexa Fluor 647 that was made in house. Lastly, 200,000 live cells per cell preparation were analyzed by flow cytometry with a BD FACSCanto Analyzer.

To analyze immune cells in blood and peripheral lymphatic organs, blood, spleens, lymph nodes (accessory axillary lymph nodes and subiliac lymph nodes) were collected from the aforementioned mice. Red blood cells in these samples were lysed with the Ammonium-Chloride-Potassium (ACK) Lysing Buffer. The remaining cells in the samples were pelleted

by a centrifugation at 300 g for 5 minutes, and then cells were stained by DAPI (3 μM), αB220-PE, αCD8-PE, αCD4-PECy7, αCD3-FITC, αFOXP3-PE, and αPD-1-Alexa Fluor 647 that was made in house. Lastly, 10,000 live cells per cell preparation were analyzed by flow cytometry with a BD FACSCanto Analyzer.

Fraction analysis of peripheral lymphocytes in healthy NOD and C57BL/6 mice

Ten-week-old female NOD mice were randomly assigned into 4 groups and treated with one dose of αPD-1-ABD-PE (5 mg/kg), a mixture of αPD-1 (scFv, 2.5 mg/kg) and ABD-PE (2.5 mg/kg), PBS, or CP (200 mg/kg) (Santa Cruz Biotechnology) intraperitoneally. These mice were euthanized 24 hours later. Blood samples and splenocytes were collected from the mice, and red blood cells in these samples were lysed with the Ammonium-Chloride-Potassium (ACK) Lysing Buffer. The remaining cells in the samples were pelleted by a centrifugation at 300 g for 5 minutes, and stained by αB220-APC (Biolegend), αCD4-PE (Biolegend), or αCD8α-PE (Santa Cruz Biotechnology, Inc). The B220+, CD4+, and CD8+ fractions in the pellets were analyzed by flow cytometry on a BD FACSCanto Analyzer. The same experiment was conducted on 10-week-old female C57BL6 mice.

Evaluation of humoral responses

Ten-week-old female NOD mice were randomly assigned into 4 groups and treated once or five times with αPD-1-ABD-PE (5 mg/kg), a mixture of αPD-1 (scFv, 2.5 mg/kg) and ABD-PE (2.5 mg/kg), PBS, or CP (200 mg/kg) (Santa Cruz Biotechnology) intraperitoneally. Two days after the last treatment, mice were immunized with 100 μg DNP-Ficoll (Biosearchtech) per mouse intraperitoneally. Five days after the immunization, serum samples were collected from these mice to determine anti-DNP IgM levels using an ELISA as previously described with some modification [46]. Specifically, serum dilutions from 100 to 10^6 folds were applied to ELISA plates pre-coated with DNP-BSA (Thermo Fisher Scientific Inc) (1 μg/well, 4 °C, overnight). After unbound IgM was washed away, a secondary antibody, anti-mouse IgM (μ chain)-HRP (Jackson ImmunoResearch) (1:5000 diluted in PBS with 1% BSA) was added into the plates. After a 1-hour incubation at room temperature, the unbound secondary antibody was washed away, and a TMB substrate (Biolegend) was added to the plates. The plates were then incubated in the dark at room temperature for 20 minutes for the colorimetric reaction to develop. The reaction was stopped with 2 M H_2SO_4. Both OD_{450} and OD_{570} (background) were measured. The same diluted serum samples were also applied to ELISA plates pre-coated with the BSA control (Sigma) (1 μg/well, 4 °C, overnight) in order to determine the non-specific binding of IgM to the plates. All other procedures were the same.

The same experiment was also performed with 10-week-old female C57BL/6 mice.

Evaluation of CTL responses

Ten-week-old female NOD mice were randomly assigned into 4 groups and treated with a single dose of αPD-1-ABD-PE (5 mg/kg), a mixture of αPD-1 (scFv, 2.5 mg/kg) and ABD-PE (2.5 mg/kg), PBS, or CP (200 mg/kg) (Santa Cruz Biotechnology) intraperitoneally. Two days later, all these mice were subcutaneously immunized with 10 nmole of TYQRTRALV (Influenza A (PR8) NP 147–155, Biomatik) per muse. The peptide was emulsified in IFA

(Sigma). Seven days after the first immunization, a second immunization was administered. Ten days after the second immunization, these mice were sacrificed, and an ELISPOT was performed with splenocytes collected from these mice as previously described[52, 53].

In a similar manner, ten-week-old female C57BL/6 mice were treated and immunized with 10 nmole of SIINFEKL (OVA 257–264). SIINFEKL-specific CTL responses were evaluated as described above.

Data availability

The authors declare that all other data supporting the findings of this study are available within the paper and its Supplementary Information. Source data for the figures and encoding genes are available in figshare at https://figshare.com/s/f14f13bf582ce99165a1 (ref[64]).

Supplementary Material

Refer to Web version on PubMed Central for supplementary material.

ACKNOWLEDGEMENTS:

We thank Xiaomin Wang and Hu Dai for their assistance in breeding mice. The flow cytometry work was conducted in the Flow Cytometry Core Facility of University of Utah. We thank Drs. Yue Zhang and Jie Wang for their review and comments on the statistical analysis of this study and Drs. Shawn Owen and Andrew Dixon for their technical assistance in antibody-related protein engineering. Simon J. Fisher was supported by grants [NS070235 and JDRF 2-SRA-2014–270-M-R]. Robert S. Fujinami was supported by grants [R01NS065714, R01NS082102, and R01NS091939]. Song Guo Zhen was supported by grants [R01AR059103, R61AR073409, and the NIH Star Award]. Peng Zhao was supported by the Graduate Research Fellowship from the University of Utah. This work was primarily supported by the University of Utah Start-up Fund, a Huntsman Cancer Institute Pilot Grant [Grant number 170301], and partially by a NIH grant [R21EB024083] to Mingnan Chen.

References

1. Bluestone JA, Herold K & Eisenbarth G Genetics, pathogenesis and clinical interventions in type 1 diabetes. Nature 464, 1293–1300 (2010). [PubMed: 20432533]
2. Atkinson MA, Eisenbarth GS & Michels AW Type 1 diabetes. Lancet 383, 69–82 (2014). [PubMed: 23890997]
3. Laurence A & Aringer M in The Autoimmune Diseases, Edn. 5th (ed. N.R.M. Rose IR) 311–318 (Elsevier, San Diego; 2014).
4. van Belle TL, Coppieters KT & von Herrath MG Type 1 diabetes: etiology, immunology, and therapeutic strategies. Physiol Rev 91, 79–118 (2011). [PubMed: 21248163]
5. Farber R, Harel A & Lublin F Novel Agents for Relapsing Forms of Multiple Sclerosis. Annu Rev Med 67, 309–321 (2016). [PubMed: 26394285]
6. Wingerchuk DM & Carter JL Multiple sclerosis: current and emerging disease-modifying therapies and treatment strategies. Mayo Clin Proc 89, 225–240 (2014). [PubMed: 24485135]
7. Kim SS, Kirou KA & Erkan D Belimumab in systemic lupus erythematosus: an update for clinicians. Therapeutic Advances in Chronic Disease 3, 11–23 (2012). [PubMed: 23251765]
8. Chatenoud L in The autoimmune diseases, Edn. 5th (ed. N.R.M. Rose IR) 1121–1145 (Elesvier, San Diego, CA, USA; 2014).
9. Elsegeiny W, Eddens T, Chen K & Kolls JK Anti-CD20 antibody therapy and susceptibility to Pneumocystis pneumonia. Infect Immun 83, 2043–2052 (2015). [PubMed: 25733518]
10. Lemtrada (alemtuzumab): Highlights of Prescribing Information. Sanofi. Bridgewater, NJ.

11. Torkildsen Ø, Myhr KM & Bø L Disease-modifying treatments for multiple sclerosis – a review of approved medications. European Journal of Neurology 23, 18–27 (2016). [PubMed: 26563094]
12. McNamara C, Sugrue G, Murray B & MacMahon PJ Current and Emerging Therapies in Multiple Sclerosis: Implications for the Radiologist, Part 2-Surveillance for Treatment Complications and Disease Progression. Am J Neuroradiol (2017).
13. Francisco LM, Sage PT & Sharpe AH The PD-1 Pathway in Tolerance and Autoimmunity. Immunological reviews 236, 219–242 (2010). [PubMed: 20636820]
14. Agata Y et al. Expression of the PD-1 antigen on the surface of stimulated mouse T and B lymphocytes. Int Immunol 8, 765–772 (1996). [PubMed: 8671665]
15. Yamazaki T et al. Expression of programmed death 1 ligands by murine T cells and APC. J Immunol 169, 5538–5545 (2002). [PubMed: 12421930]
16. Joller N, Peters A, Anderson AC & Kuchroo VK Immune checkpoints in central nervous system autoimmunity. Immunol Rev 248, 122–139 (2012). [PubMed: 22725958]
17. Liang SC et al. Regulation of PD-1, PD-L1, and PD-L2 expression during normal and autoimmune responses. Eur J Immunol 33, 2706–2716 (2003). [PubMed: 14515254]
18. Zhu B et al. Differential role of programmed death-ligand 1 [corrected] and programmed death-ligand 2 [corrected] in regulating the susceptibility and chronic progression of experimental autoimmune encephalomyelitis. J Immunol 176, 3480–3489 (2006). [PubMed: 16517716]
19. Salama AD et al. Critical role of the programmed death-1 (PD-1) pathway in regulation of experimental autoimmune encephalomyelitis. J Exp Med 198, 71–78 (2003). [PubMed: 12847138]
20. Latchman YE et al. PD-L1-deficient mice show that PD-L1 on T cells, antigen-presenting cells, and host tissues negatively regulates T cells. Proc Natl Acad Sci U S A 101, 10691–10696 (2004). [PubMed: 15249675]
21. Okazaki T, Chikuma S, Iwai Y, Fagarasan S & Honjo T A rheostat for immune responses: the unique properties of PD-1 and their advantages for clinical application. Nat Immunol 14, 1212–1218 (2013). [PubMed: 24240160]
22. Keir ME, Butte MJ, Freeman GJ & Sharpe AH PD-1 and its ligands in tolerance and immunity. Annu Rev Immunol 26, 677–704 (2008). [PubMed: 18173375]
23. Fife BT et al. Interactions between PD-1 and PD-L1 promote tolerance by blocking the TCR-induced stop signal. Nat Immunol 10, 1185–1192 (2009). [PubMed: 19783989]
24. Godwin JL et al. Nivolumab-induced autoimmune diabetes mellitus presenting as diabetic ketoacidosis in a patient with metastatic lung cancer. J Immunother Cancer 5, 40 (2017). [PubMed: 28515940]
25. Ansari MJ et al. The programmed death-1 (PD-1) pathway regulates autoimmune diabetes in nonobese diabetic (NOD) mice. J Exp Med 198, 63–69 (2003). [PubMed: 12847137]
26. Hughes J et al. Precipitation of autoimmune diabetes with anti-PD-1 immunotherapy. Diabetes Care 38, e55–57 (2015). [PubMed: 25805871]
27. Zhao P et al. An Anti-Programmed Death-1 Antibody (αPD-1) Fusion Protein That Self-Assembles into a Multivalent and Functional αPD-1 Nanoparticle. Molecular Pharmaceutics 14, 1494–1500 (2017). [PubMed: 28343398]
28. Levy OE et al. Novel exenatide analogs with peptidic albumin binding domains: potent anti-diabetic agents with extended duration of action. PLoS One 9, e87704 (2014). [PubMed: 24503632]
29. Wang P et al. An albumin binding polypeptide both targets cytotoxic T lymphocyte vaccines to lymph nodes and boosts vaccine presentation by dendritic cells. Theranostics **(In press)**.
30. Weldon JE et al. A recombinant immunotoxin against the tumor-associated antigen mesothelin reengineered for high activity, low off-target toxicity, and reduced antigenicity. Mol Cancer Ther 12, 48–57 (2013). [PubMed: 23136186]
31. Onda M et al. Recombinant immunotoxin against B-cell malignancies with no immunogenicity in mice by removal of B-cell epitopes. Proc Natl Acad Sci U S A 108, 5742–5747 (2011). [PubMed: 21436054]
32. Chen H et al. Chemical Conjugation of Evans Blue Derivative: A Strategy to Develop Long-Acting Therapeutics through Albumin Binding. Theranostics 6, 243–253 (2016). [PubMed: 26877782]

33. Hassan R, Alewine C & Pastan I New Life for Immunotoxin Cancer Therapy. Clin Cancer Res 22, 1055–1058 (2016). [PubMed: 26463707]
34. Jonsson A, Dogan J, Herne N, Abrahmsen L & Nygren PA Engineering of a femtomolar affinity binding protein to human serum albumin. Protein Eng Des Sel 21, 515–527 (2008). [PubMed: 18499681]
35. Yamazaki T et al. Blockade of B7-H1 on macrophages suppresses CD4+ T cell proliferation by augmenting IFN-gamma-induced nitric oxide production. J Immunol 175, 1586–1592 (2005). [PubMed: 16034097]
36. Brinkmann U in Antibody Engineering. (eds. Kontermann R & Dübel S) 181–189 (Springer Berlin Heidelberg, Berlin, Heidelberg; 2010).
37. Hirano F et al. Blockade of B7-H1 and PD-1 by monoclonal antibodies potentiates cancer therapeutic immunity. Cancer Res 65, 1089–1096 (2005). [PubMed: 15705911]
38. Bera TK, Onda M, Kreitman RJ & Pastan I An improved recombinant Fab-immunotoxin targeting CD22 expressing malignancies. Leukemia research 38, 1224–1229 (2014). [PubMed: 25127689]
39. Fife BT et al. Insulin-induced remission in new-onset NOD mice is maintained by the PD-1-PD-L1 pathway. J Exp Med 203, 2737–2747 (2006). [PubMed: 17116737]
40. Brode S, Raine T, Zaccone P & Cooke A Cyclophosphamide-induced type-1 diabetes in the NOD mouse is associated with a reduction of CD4+CD25+Foxp3+ regulatory T cells. J Immunol 177, 6603–6612 (2006). [PubMed: 17082572]
41. Wang J et al. Establishment of NOD-Pdcd1−/− mice as an efficient animal model of type I diabetes. Proc Natl Acad Sci U S A 102, 11823–11828 (2005). [PubMed: 16087865]
42. Wang Y et al. Neuropilin-1 modulates interferon-gamma-stimulated signaling in brain microvascular endothelial cells. J Cell Sci 129, 3911–3921 (2016). [PubMed: 27591257]
43. Rangachari M & Kuchroo VK Using EAE to better understand principles of immune function and autoimmune pathology. J Autoimmun 45, 31–39 (2013). [PubMed: 23849779]
44. Schreiner B, Bailey SL, Shin T, Chen L & Miller SD PD-1 ligands expressed on myeloid-derived APC in the CNS regulate T-cell responses in EAE. Eur J Immunol 38, 2706–2717 (2008). [PubMed: 18825752]
45. Massilamany C, Upadhyaya B, Gangaplara A, Kuszynski C & Reddy J Detection of autoreactive CD4 T cells using major histocompatibility complex class II dextramers. BMC immunology 12, 40 (2011). [PubMed: 21767394]
46. Turner MJ et al. Immune status following alemtuzumab treatment in human CD52 transgenic mice. J Neuroimmunol 261, 29–36 (2013). [PubMed: 23759318]
47. Sharon R, McMaster PR, Kask AM, Owens JD & Paul WE DNP-Lys-ficoll: a T-independent antigen which elicits both IgM and IgG anti-DNP antibody-secreting cells. J Immunol 114, 1585–1589 (1975). [PubMed: 1091706]
48. Zhang Q & Vignali DA Co-stimulatory and Co-inhibitory Pathways in Autoimmunity. Immunity 44, 1034–1051 (2016). [PubMed: 27192568]
49. Sharpe AH & Pauken KE The diverse functions of the PD1 inhibitory pathway. Nat Rev Immunol 18, 153–167 (2018). [PubMed: 28990585]
50. Davidson A & D'iamond B in The Autoimmune Diseases, Edn. Fifth Edition (ed. N.R.M. Rose IR) 19–37 (Elsevier Inc, San Diego, CA, USA; 2014).
51. Kasagi S et al. In vivo-generated antigen-specific regulatory T cells treat autoimmunity without compromising antibacterial immune response. Sci Transl Med 6, 241ra278 (2014).
52. Dong S, Xu T, Wang P, Zhao P & Chen M Engineering of a self-adjuvanted iTEP-delivered CTL vaccine. Acta pharmacologica Sinica 38, 914–923 (2017). [PubMed: 28414197]
53. Dong S, Xu T, Zhao P, Parent KN & Chen M A Comparison Study of iTEP Nanoparticle-Based CTL Vaccine Carriers Revealed a Surprise Relationship between the Stability and Efficiency of the Carriers. Theranostics 6, 666–678 (2016). [PubMed: 27022414]
54. Zimmerman T et al. Simultaneous metal chelate affinity purification and endotoxin clearance of recombinant antibody fragments. Journal of immunological methods 314, 67–73 (2006). [PubMed: 16824538]

55. Hunter SA & Cochran JR Cell-Binding Assays for Determining the Affinity of Protein-Protein Interactions: Technologies and Considerations. Methods in enzymology 580, 21–44 (2016). [PubMed: 27586327]
56. Shalem O et al. Genome-scale CRISPR-Cas9 knockout screening in human cells. Science (New York, N.Y.) 343, 84–87 (2014).
57. Pear WS, Nolan GP, Scott ML & Baltimore D Production of high-titer helper-free retroviruses by transient transfection. Proceedings of the National Academy of Sciences of the United States of America 90, 8392–8396 (1993). [PubMed: 7690960]
58. Zhang Y, Huo M, Zhou J & Xie S PKSolver: An add-in program for pharmacokinetic and pharmacodynamic data analysis in Microsoft Excel. Computer methods and programs in biomedicine 99, 306–314 (2010). [PubMed: 20176408]
59. Zhao P et al. An Anti-Programmed Death-1 Antibody (alphaPD-1) Fusion Protein That Self-Assembles into a Multivalent and Functional alphaPD-1 Nanoparticle. Molecular pharmaceutics 14, 1494–1500 (2017). [PubMed: 28343398]
60. Gregori S, Giarratana N, Smiroldo S & Adorini L Dynamics of pathogenic and suppressor T cells in autoimmune diabetes development. Journal of immunology (Baltimore, Md. : 1950) 171, 4040–4047 (2003).
61. Chitnis T et al. Effect of targeted disruption of STAT4 and STAT6 on the induction of experimental autoimmune encephalomyelitis. Journal of Clinical Investigation 108, 739–747 (2001). [PubMed: 11544280]
62. McMahon EJ, Bailey SL, Castenada CV, Waldner H & Miller SD Epitope spreading initiates in the CNS in two mouse models of multiple sclerosis. Nature medicine 11, 335–339 (2005).
63. Pino PA & Cardona AE Isolation of brain and spinal cord mononuclear cells using percoll gradients. Journal of visualized experiments : JoVE (2011).
64. Zhao P & al., e. Depletion of PD-1-positive cells ameliorates autoimmune disease. figshare https://figshare.com/s/f14f13bf582ce99165a1 (2019).

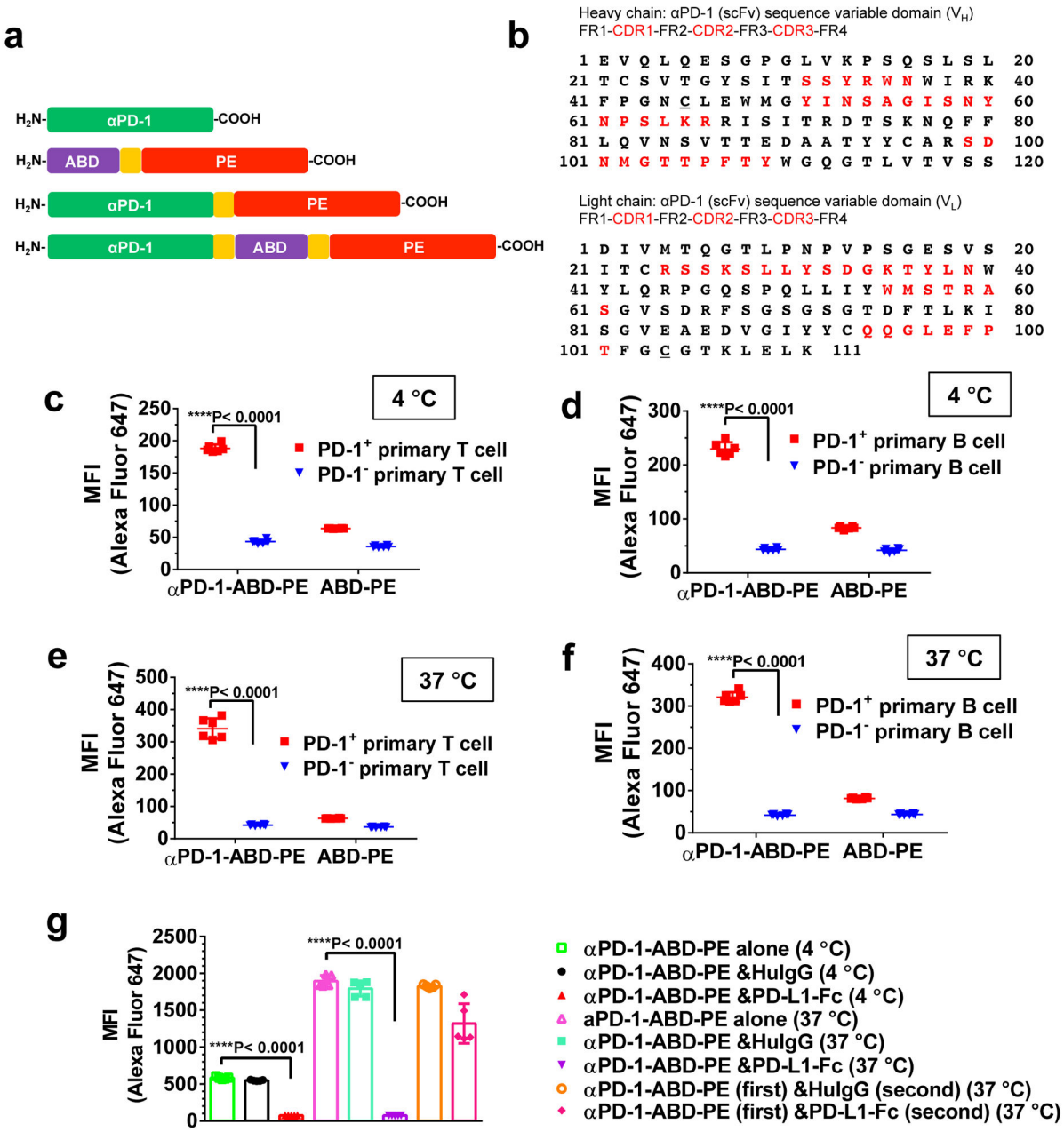

Figure 1. αPD-1-ABD-PE consisting of αPD-1, ABD, and PE specifically binds with and enters PD-1$^+$ lymphocytes.

(a) The sequential configurations of the functional domains, αPD-1, ABD, and PE, in αPD-1, ABD-PE, αPD-1-PE, and αPD-1-ABD-PE. The linker, $(GGGGS)_3$, is shown as an orange box. **(b)** The amino acid sequences of αPD-1 V_H and V_L with their framework regions (FRs) and complementarity-determining regions (CDRs) highlighted with red text. Two mutations were introduced in the V_H and V_L, respectively. The two mutations are underlined, V_H: R45C; V_L: G104C. **(c)** The mean fluorescence intensity (MFI) of PD-1$^+$ and PD-1$^-$ primary T cells after the cells were incubated with Alexa Fluor 647-labeled αPD-1-ABD-PE or Alexa Fluor 647-labeled ABD-PE at 4°C for 30 minutes. The cells were

collected from C57BL/6 mice. The MFI means and their standard deviations (SDs) are indicated (N=6 biologically independent samples; unpaired two-sided t-test). The MFI was obtained by flow cytometry. **(d)** The MFI of PD-1^+ and PD-1^- primary B cells after the cells were incubated with the labeled αPD-1-ABD-PE or the labeled ABD-PE at 4°C for 30 minutes. The cells were collected from C57BL/6 mice. The MFI means and their SDs are indicated (N=6 biologically independent samples, unpaired two-sided t-test). **(e)** The MFI of PD-1^+ and PD-1^- primary T cells after the cells were incubated with the labeled αPD-1-ABD-PE or the labeled ABD-PE at 37°C for 30 minutes. The cells were collected from C57BL/6 mice. The MFI means and their SDs are indicated (N=6 biologically independent samples; unpaired two-sided t-test). **(f)** The MFI of PD-1^+ and PD-1^- primary B cells after the cells were incubated with the labeled αPD-1-ABD-PE or the labeled ABD-PE at 37°C for 30 minutes. The cells were collected from C57BL/6 mice. The MFIs and their SDs are indicated (N=6 biologically independent samples; unpaired two-sided t-test). **(g)** The MFI of EL4 cells after the cells were incubated with the labeled αPD-1-ABD-PE under the conditions noted in the figure. The MFIs and their SDs are indicated (N=6 biologically independent samples; unpaired two-sided t-test). Studies described in the panels c-g were repeated twice with similar results. Data of one repeat is shown here.

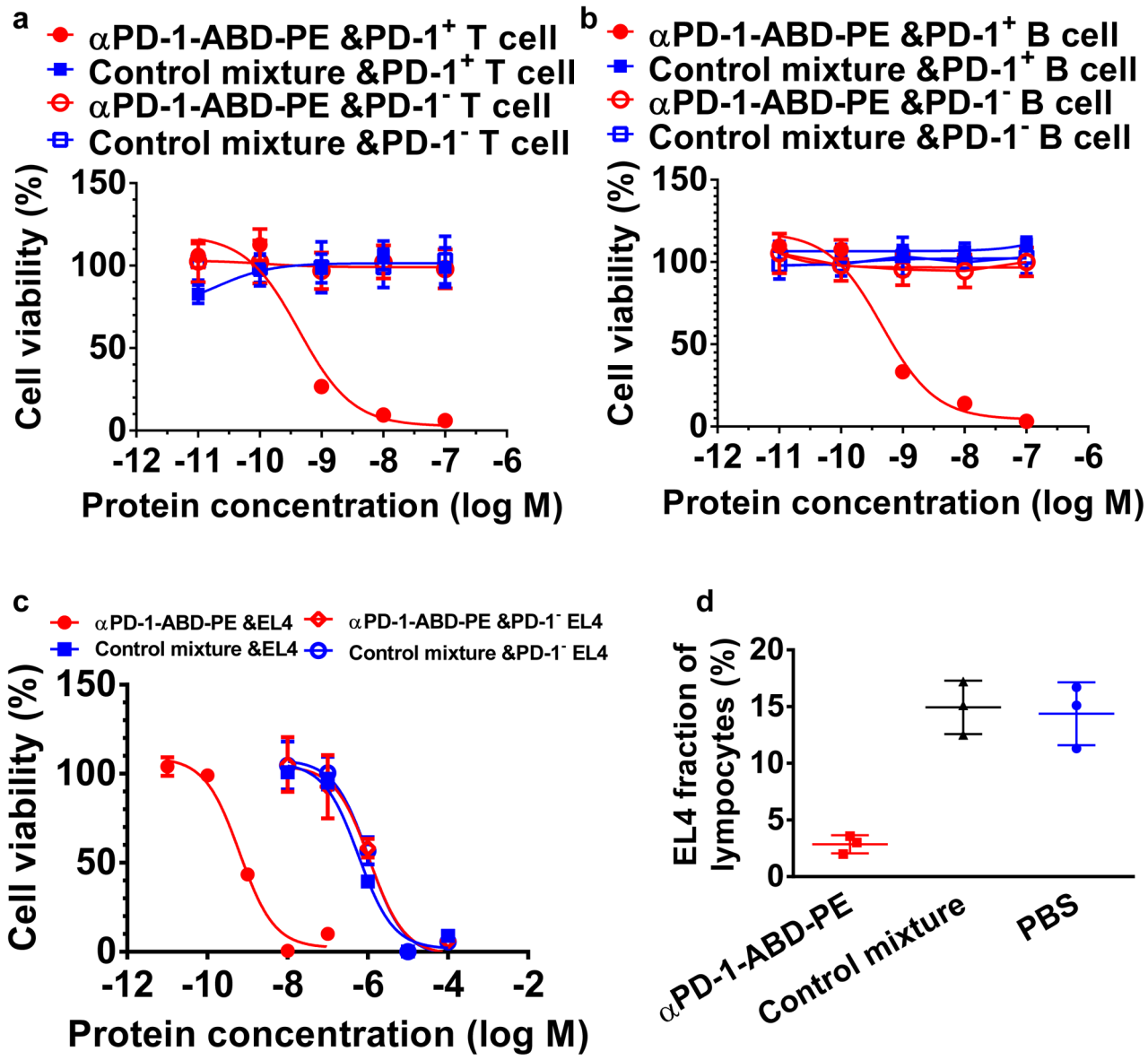

Figure 2. αPD-1-ABD-PE is selectively toxic to PD-1$^+$ cells *in vitro* and *in vivo*.

(a) The relative viability of PD-1$^+$ and PD-1$^-$ primary T cells after they were incubated with αPD-1-ABD-PE or a control mixture of αPD-1 and ABD-PE for 72 hours. The mean viabilities and their SDs at different concentrations of αPD-1-ABD-PE and the control mixture were shown. The viability data of PD-1$^+$ primary T cells after the αPD-1-ABD-PE treatment were fitted to a Sigmoidal dose-response model and the IC_{50} was obtained through the fitting (N=6 biologically independent samples). The cells were collected from C57BL/6 mice. **(b)** The relative viability of PD-1$^+$ and PD-1$^-$ primary B cells after they were incubated with αPD-1-ABD-PE or a control mixture of αPD-1 and ABD-PE for 72 hours. The mean viabilities and their SDs at different concentrations of αPD-1-ABD-PE and the control mixture were shown (N=6 biologically independent samples). The cells were collected from C57BL/6 mice. **(c)** The relative viability of wildtype EL4 and PD-1$^-$ EL4

cells after they were incubated with αPD-1-ABD-PE or a control mixture of αPD-1 and ABD-PE for 72 hours. The mean viabilities and their SDs at different concentrations of αPD-1-ABD-PE and the control mixture were shown and fitted to a Sigmoidal dose-response model (N=6 biologically independent samples). **(d)** The fractions of transferred EL4 cells among lymphocytes. These lymphocytes were collected from mice at 72 hours after these mice were treated with αPD-1-ABD-PE, a control mixture of αPD-1 and ABD-PE, or PBS. The mean faction values and their SDs are indicated (N=3 mice). All studies described in this figure were repeated twice with similar results. Data of one repeat is shown here.

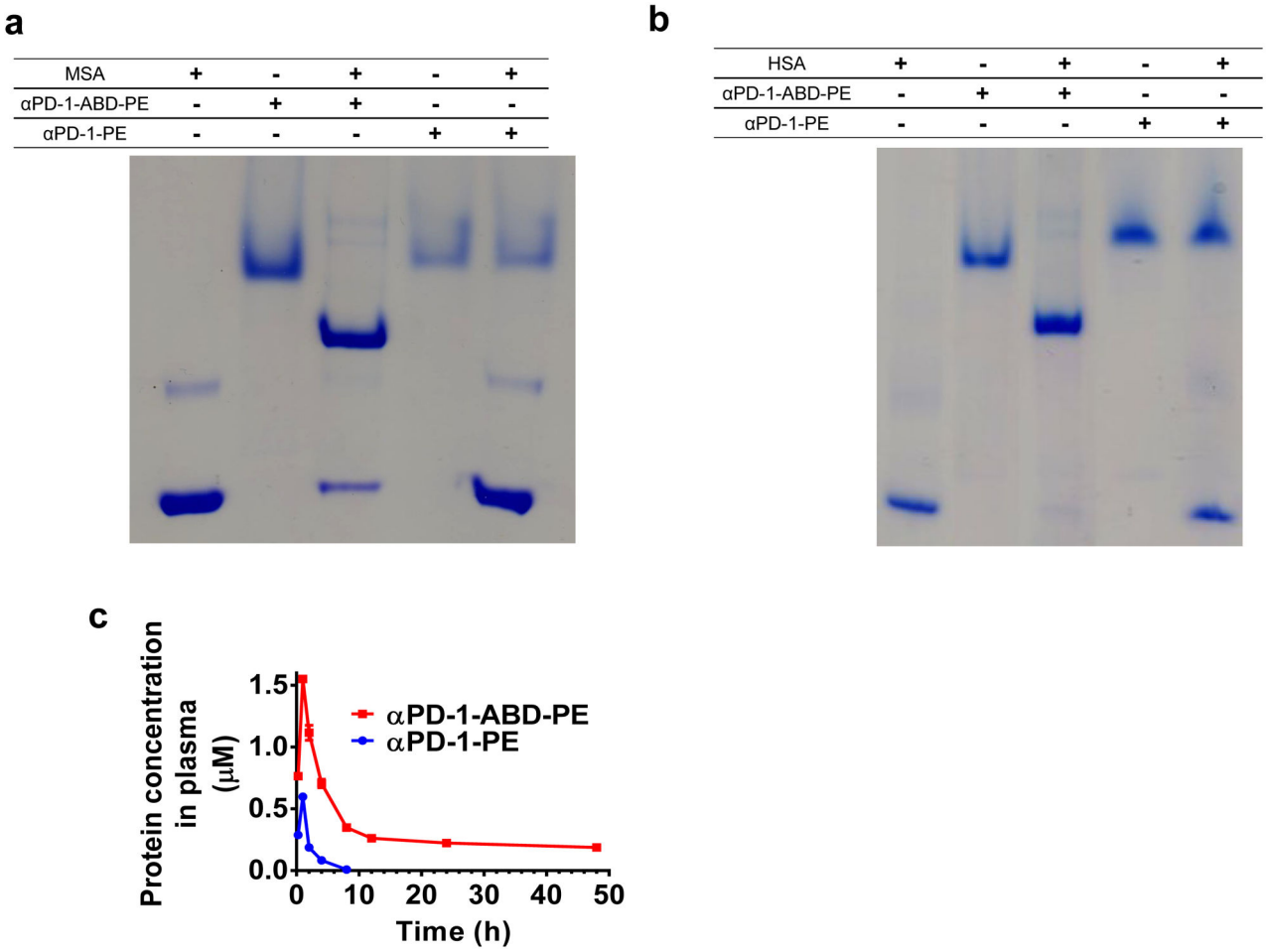

Figure 3. αPD-1-ABD-PE binds with albumin and has enhanced plasma exposure.

(a) A photo of native PAGE gel that demonstrates the association between αPD-1-ABD-PE and MSA. αPD-1-ABD-PE and MSA were mixed the 1-to-1 ratio. αPD-1-PE and MSA were also mixed the 1-to-1 ratio. **(b)** A photo of native PAGE gel that demonstrates the association between αPD-1-ABD-PE and HSA. αPD-1-ABD-PE and HSA were mixed at the 1-to-1 ratio. αPD-1-PE and HSA were also mixed at the 1-to-1 ratio. Studies described in the panels a-b were repeated independently at least three times showing similar results. The representative data were shown here. **(c)** The plasma concentration versus time profiles of αPD-1-ABD-PE and αPD-1-PE after the two protein were intraperitoneally injected into mice at the same dose 5 nmol per mouse (N=3 biologically independent samples: error bars represent SD with the measure of center as mean values). The PK data was analyzed using non-compartmental model. Each dot represents a plasma concentration value at a given time points.

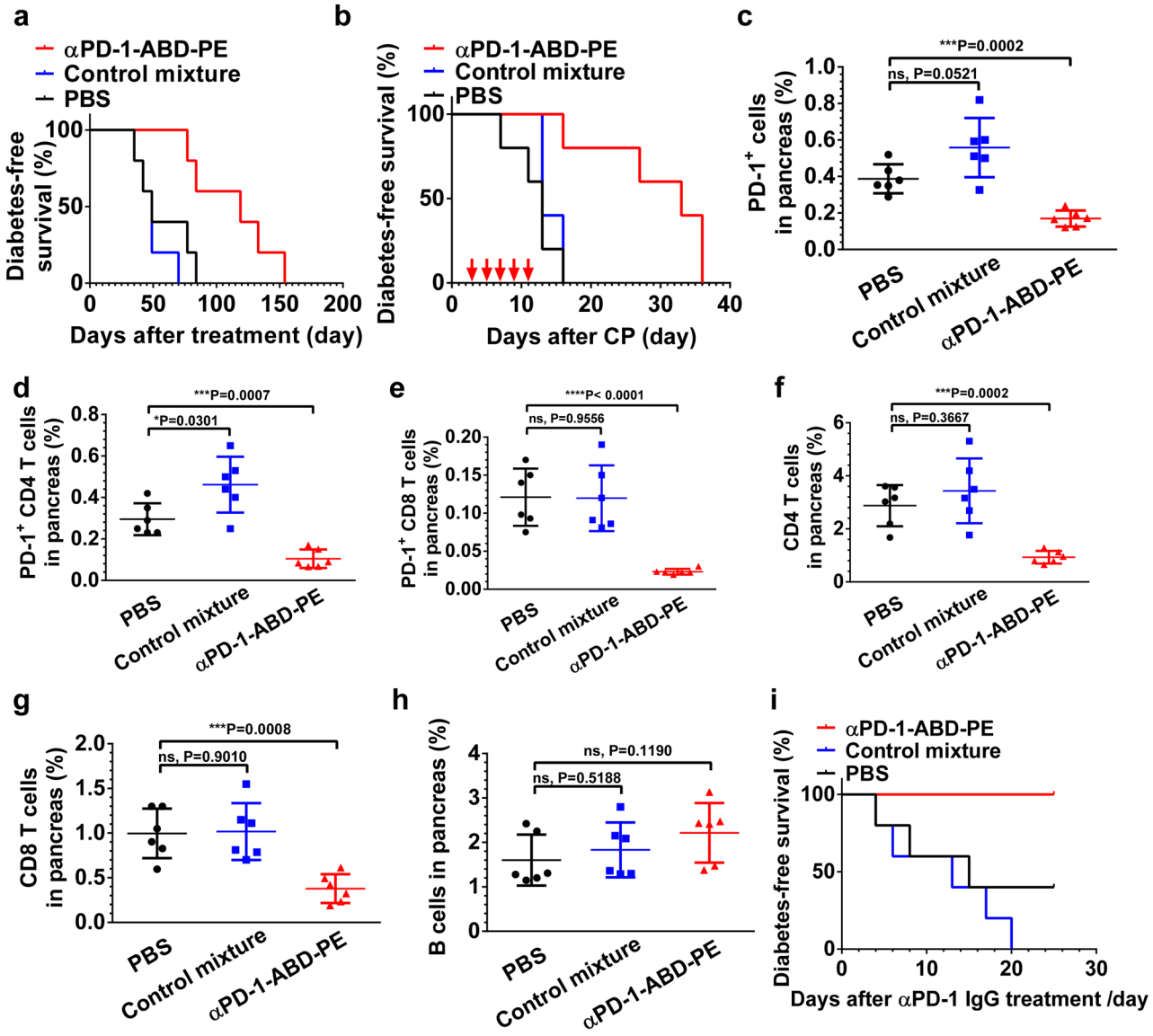

Figure 4. Administration of αPD-1-ABD-PE delays the onset of T1D.

(a) The diabetes-free survival of NOD mice that were treated with αPD-1-ABD-PE, a control mixture of αPD-1 and ABD-PE, or PBS weekly since there mice were 12 weeks old (N=5 mice). **(b)** The diabetes-free survival of NOD mice that were treated five times with αPD-1-ABD-PE, a control mixture of αPD-1 and ABD-PE, or PBS (N=5 mice). The arrows indicate the five dosing dates of the treatments. Before these treatments, all of these mice were treated with CP at day 0. **(c)** The fraction of PD-1$^+$ cells among collected pancreatic cells from 18-week old NOD mice after these mice were treated with one dose of αPD-1-ABD-PE, a control mixture of αPD-1 and ABD-PE, or PBS. Each dot represents the fraction value of a single mouse. The fraction means and their SDs are indicated. (N=6 mice; unpaired two-sided t-test). **(d)** The fraction of PD-1$^+$ CD4 T cells among the pancreatic cells described in (c). Each dot represents the fraction result of a single mouse. The fraction means and their SDs are indicated. (N=6 mice; unpaired two-sided t-test). **(e)** The fraction of

PD-1$^+$ CD8 T cells among the pancreatic cells described in (c). Each dot represents the fraction result of a single mouse. The fraction means and their SDs are indicated. (N=6 mice; unpaired two-sided t-test). **(f)** The fraction of CD4 T cells among the pancreatic cells described in (c). Each dot represents the fraction result of a single mouse. The fraction means and their SDs are indicated. (N=6 mice; unpaired two-sided t-test). **(g)** The fraction of CD8 T cells among the pancreatic cells described in (c). Each dot represents the fraction result of a single mouse. The fraction means and their SDs are indicated. (N=6 mice; unpaired two-sided t-test). **(h)** The fraction of B cells among the pancreatic cells described in (c). Each dot represents the fraction result of a single mouse. The fraction means and their SDs are indicated. (N=6 mice; unpaired two-sided t-test). **(i)** The diabetes-free survival of NOD mice that were first treated with αPD-1-ABD-PE, a control mixture of αPD-1 and ABD-PE, or PBS, and then with αPD-1 (full IgG). (N=5 mice; unpaired two-sided t-test) The survival of αPD-1-ABD-PE treated mice is significantly different to PBS and the control mixture treated mice (P=0.0494 and P=0.0018, respectively). All studies described in this figure were repeated twice with similar results. Data of one repeat is shown here.

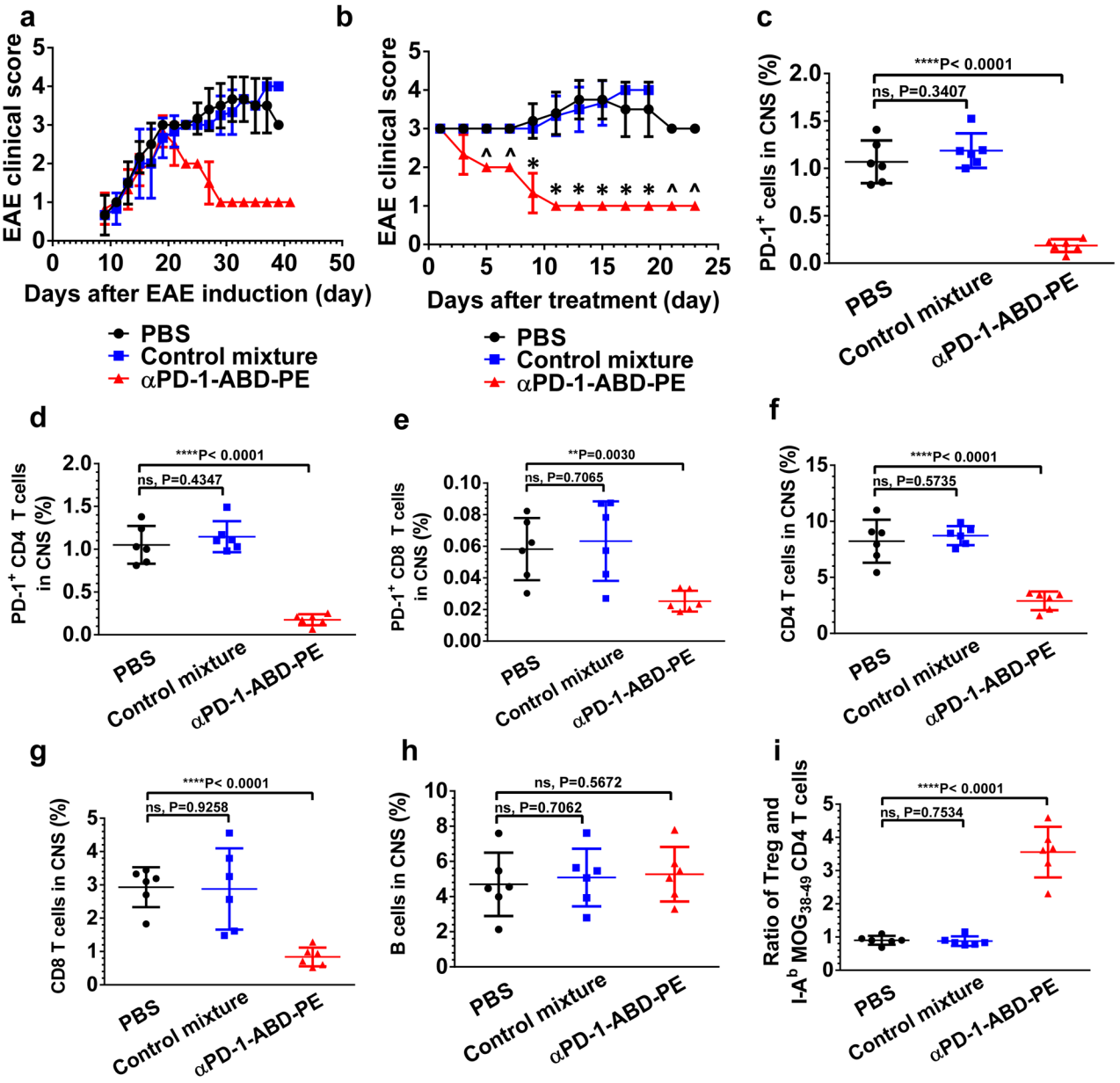

Figure 5. Administration of αPD-1-ABD-PE ameliorates symptoms in mice with clinically EAE.

(a) The clinical score changes of the mice with EAE that were treated with one dose of αPD-1-ABD-PE, a control mixture of αPD-1 and ABD-PE, or PBS. The shown data are mean scores and their standard deviations at each observation time point after the induction of EAE. (N=6 mice). The X-axis indicates the number of days after EAE induction. **(b)** The clinical score changes of the mice described in (a). The shown data are mean scores and their standard deviations at each observation time point after the treatments. The mean clinical score of the αPD-1-ABD-PE group was different from the score of the PBS group since day 5 post treatment (*P<0.0002; unpaired two-sided t-test). "^" was used to denote those days when the mean clinical scores of the two groups were apparently different however t-test could not be conducted because the scores of the both groups have no

variation. The X-axis indicates the number of days since an individual mouse received treatments. The experiment described in "**a**" and "**b**" was repeated trice and the data of one repeat is shown here. **(c)** The fraction of PD-1^+ cells among the collected mononuclear cells from the CNS of the mice that were treated with one dose of αPD-1-ABD-PE, a control mixture of αPD-1 and ABD-PE, or PBS. Each dot represents the fraction result of a single mouse. The fraction means and their SDs are indicated. (N=6 mice; unpaired two-sided t-test). **(d)** The fraction of PD-1^+ CD4 T cells among the mononuclear cells described in (c). Each dot represents the fraction result of a single mouse. The fraction means and their SDs are indicated (N=6 mice; unpaired two-sided t-test). **(e)** The fraction of PD-1^+ CD8 T cells among the mononuclear cells described in (c). Each dot represents the fraction result of a single mouse. The fraction means and their SDs are indicated (N=6 mice; unpaired two-sided t-test). **(f)** The fraction of CD4 T cells among the mononuclear cells described in (c). Each dot represents the fraction result of a single mouse. The fraction means and their SDs are indicated (N=6 mice; unpaired two-sided t-test). **(g)** The fraction of CD8 T cells among the mononuclear cells described in (c). Each dot represents the fraction result of a single mouse. The fraction means and their SDs are indicated (N=6 mice; unpaired two-sided t-test). **(h)** The fraction of B cells among the mononuclear cells described in (c). Each dot represents the fraction result of a single mouse. The fraction means and their SDs are indicated (N=6 mice; unpaired two-sided t-test). **(i)** The ratios between Tregs and the MOG-specific CD4 T cells in the mononuclear cells described in (c). Each dot represents the ratio result of a single mouse. The fraction means and their SDs are indicated (N=6 mice; unpaired two-sided t-test). All studies described in this figure were repeated twice with similar results. Data of one repeat is shown here.

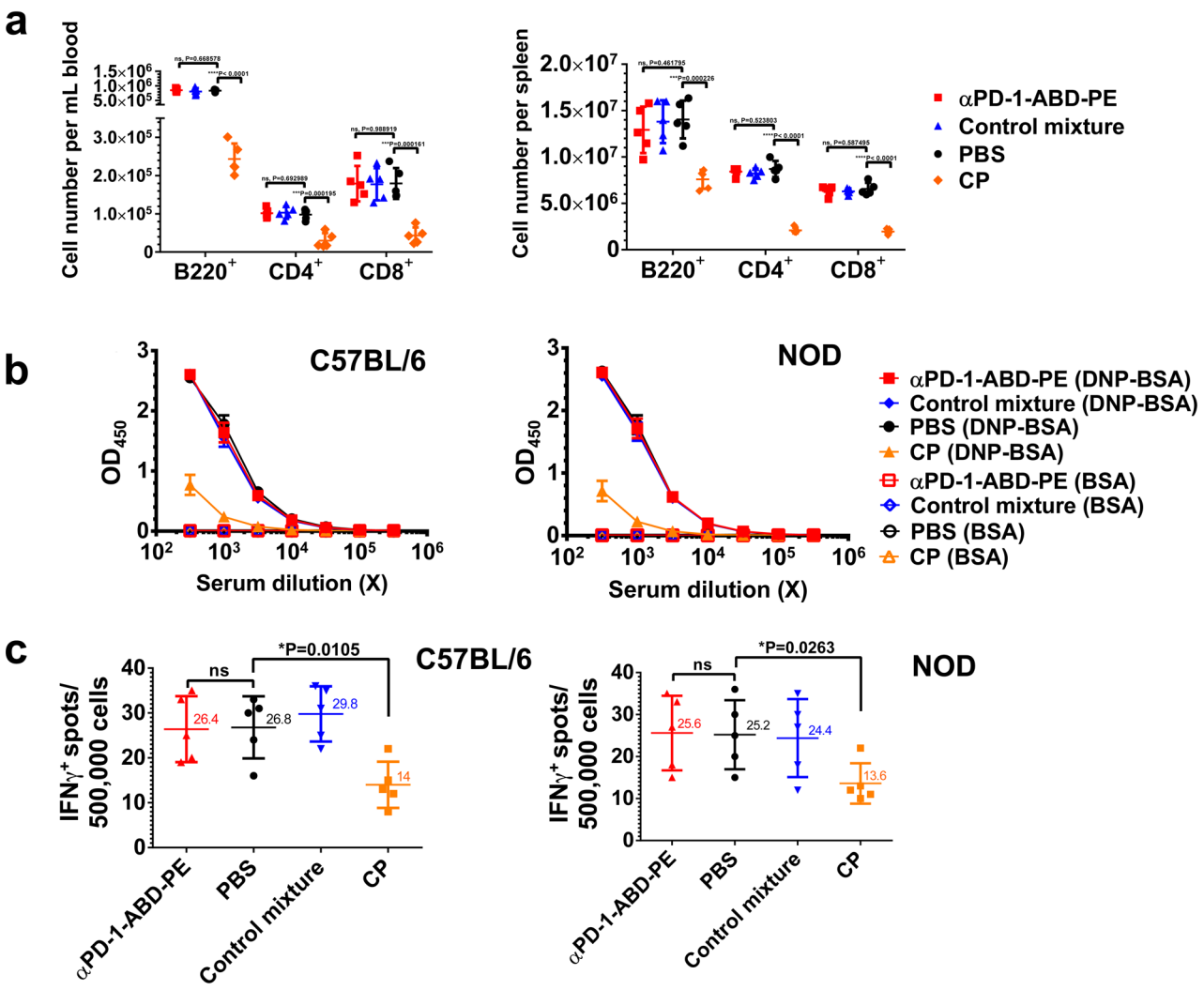

Figure 6. Administration of αPD-1-ABD-PE does not affect normal adaptive immune responses.

(a) B220+, CD4+, CD8+ cell numbers in blood and spleens in the C57BL/6 mice that were treated with one dose of αPD-1-ABD-PE, a control mixture of αPD-1 and ABD-PE, PBS, or CP. The cell number means and their SDs are indicated (N=6 mice; unpaired two-sided t-test). **(b)** ELISA results of the anti-DNP humoral responses in the C57BL/6 and NOD mice that that were pre-treated with one dose of αPD-1-ABD-PE, a control mixture of αPD-1 and ABD-PE, PBS, or CP. The results were measured by OD_{450} after a background OD_{570} subtraction. The mean ± SD of OD_{450} for the serum samples at indicated dilutions were shown. The same samples were loaded into both DNP-BSA-coated and BSA-coated (control) ELISA plates, separately. The materials used to coat the plates are written in the parentheses. (N=6 mice). **(c)** ELISPOT results of the CTL responses in the C57BL/6 and NOD mice that were treated with one dose of αPD-1-ABD-PE, a control mixture of αPD-1 and ABD-PE, PBS, or CP. The Y-axis represents the number of IFN-γ-positive spots resulting from the 500,000 splenocytes collected from these treated mice. The means and their SDs of the spot numbers are indicated. (N=6 mice; unpaired two-sided t-test; for the data of C57BL/6 mice, ns, not significant, P=0.9314 unpaired t-test; for the data of NOD

mice, ns, not significant, P=0.9429). All studies described in this figure were repeated at least twice with similar results. Data of one repeat is shown here.

Table 1.

Summary of key PK parameters derived from non-compartmental analysis

Sample	αPD-1-ABD-PE (Mean ± SD)	αPD-1-PE (Mean ± SD)
CL (mL/hr)	0.14 ± 0.01	4.05 ± 0.02
AUC (mM.Hr)	35.63 ± 2.31	1.23 ± 0.01
$\mathbf{t_{(1/2/)}}$ (Hr)	76.35 ± 9.13	1.34 ± 0.02
$\mathbf{V_d}$ (mL)	15.43 ± 1.06	7.82 ± 0.15